RadioGraphics

From the Archives of the AFIP

Neoplasms of the Urinary Bladder: Radiologic-Pathologic Correlation[1]

Jade J. Wong-You–Cheong, MD • Paula J. Woodward, MD
Maria A. Manning, MD • Isabell A. Sesterhenn, MD

CME FEATURE

See accompanying test at http://www.rsna.org/education/rg_cme.html

LEARNING OBJECTIVES FOR TEST 6

After reading this article and taking the test, the reader will be able to:

- Describe the pathologic classification of bladder neoplasms.
- Discuss the pathogenesis of and risk factors for bladder neoplasms.
- List the imaging characteristics of the various bladder neoplasms, with emphasis on distinguishing features.

TEACHING POINTS

See last page

In the United States, primary bladder neoplasms account for 2%–6% of all tumors, with bladder cancer ranked as the fourth most common malignancy. Ninety-five percent of bladder neoplasms arise from the epithelium; the most common subtype is urothelial carcinoma, which accounts for 90% of cases. Squamous cell carcinoma accounts for 2%–15%, with rates varying widely according to geographic location. Adenocarcinoma (primary bladder, urachal, or metastatic) represents less than 2%. Bladder cancer typically occurs in men aged 50–70 years and is related to smoking or occupational exposure to carcinogens. Most urothelial neoplasms are low-grade papillary tumors, which tend to be multifocal and recur but have a relatively good prognosis. High-grade invasive tumors are less common and have a much poorer prognosis. Squamous cell carcinoma and adenocarcinoma occur in the setting of chronic bladder infection and irritation. Mesenchymal tumors represent the remaining 5% of bladder tumors, with the most common types being rhabdomyosarcoma, typically seen in children, and leiomyosarcoma, a disease of adults. Rarer mesenchymal tumors include paraganglioma, lymphoma, leiomyoma, and solitary fibrous tumor. Although imaging findings are not specific for these tumors, patterns of growth and tumor characteristics may allow differentiation. For accurate staging, computed tomography and magnetic resonance imaging are the modalities of choice.

Abbreviation: MIBG = metaiodobenzylguanidine

RadioGraphics 2006; 26:553–580 • **Published online** 10.1148/rg.262055172 • **Content Codes:** CT GU MR

[1]From the Department of Diagnostic Radiology, University of Maryland School of Medicine, 22 S Greene St, Baltimore, MD 21201-1595 (J.J.W.); and the Department of Radiologic Pathology, Armed Forces Institute of Pathology, Washington, DC (P.J.W., M.A.M., I.A.S.). Received September 19, 2005; revision requested September 29; revision received and accepted October 31. All authors have no financial relationships to disclose. **Address correspondence to** J.J.W. (e-mail: *jwong@umm.edu*).

Introduction

In the United States, primary bladder neoplasms account for 2%–6% of all tumors, with bladder cancer ranked as the fourth most common malignancy (1). Tumors may arise from the epithelial surface or any of the various layers of the bladder wall. To understand the histologic varieties and radiologic appearance of these tumors, it is important to review the histologic components of the normal bladder.

The bladder wall consists of four layers (Fig 1). The lumen is lined by uroepithelium, which consists of three to seven layers of stratified flat cells. The more superficial layers contain large cells with large nuclei and acidophilic cytoplasm and small amounts of neutral mucin. These cells are flexible and can change shape from cuboidal to flattened as the bladder distends, hence the term *transitional epithelium*. The second layer underneath the epithelium is the lamina propria, which is very vascular. Deep to the lamina propria is the third layer, consisting of bundles of smooth detrusor muscle (muscularis propria). The detrusor muscle is a complex network of interlacing smooth muscle fibers. The inner and outer muscle fibers tend to be oriented in a longitudinal fashion, but distinct layers are usually not discernible. Fibers from the detrusor muscle merge with the prostate capsule or anterior vagina and pelvic floor muscles. A fourth adventitial layer is formed by connective tissue. A serosal covering, formed by the peritoneum, is present only over the bladder dome. The bladder is within the extraperitoneal space and is surrounded by pelvic fat.

Bladder neoplasms can arise from any of the bladder layers. They are broadly classified as either epithelial or nonepithelial (mesenchymal), with over 95% being epithelial (Table 1) (1). Epithelial tumors with differentiation toward normal urothelium are urothelial. The term *urothelial carcinoma* is now preferred over *transitional carcinoma*. Urothelial tumors exhibit a spectrum of neoplasia ranging from a benign papilloma through carcinoma in situ to invasive carcinoma (1). Other primary epithelial tumors include squamous carcinoma and adenocarcinoma in decreasing order of frequency. Much rarer epithelial tumors are small cell/neuroendocrine carcinoma, carcinoid, and melanoma. Because epithelial masses derive from the most superficial layer of the bladder wall, they often appear as irregular, intraluminal filling defects.

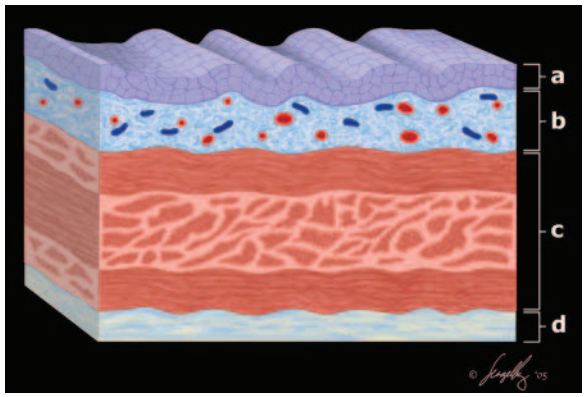

Figure 1. Normal bladder wall. Diagram shows the urothelium *(a)*, lamina propria *(b)*, muscularis propria (detrusor muscle) *(c)*, and adventitia *(d)*.

Neoplasms derived from mesenchymal tissue differentiate toward muscle, nerve, cartilage, fat, fibrous tissue, and blood vessels. Benign tumors include leiomyoma, paraganglioma, fibroma, plasmacytoma, hemangioma, solitary fibrous tumor, neurofibroma, and lipoma. Malignant tumors include rhabdomyosarcoma, leiomyosarcoma, lymphoma, and osteosarcoma. Mesenchymal tumors arise from the submucosal portion of the bladder wall and therefore more often appear as smooth intramural lesions.

Over 80% of patients with bladder cancer have hematuria, which is typically macroscopic and painless (2). Patients presenting with macroscopic hematuria should undergo thorough evaluation to determine the cause (3). Microscopic hematuria, defined as three or more red blood cells per high-power field from two of three urine specimens, is usually an incidental finding. It may portend significant underlying disease such as bladder or renal cancer or may be of little clinical importance. According to the American Urological Association guidelines, patients with asymptomatic microscopic hematuria who have no evidence of primary renal disease and in whom benign causes such as menstruation, exercise, trauma, and infection have been excluded require urologic work-up (4). The guidelines recommend upper tract imaging evaluation with computed tomography (CT) or excretory urography and bladder evaluation with cystoscopy (4).

Table 1
Neoplasms of the Urinary Bladder

Epithelial neoplasms
Benign neoplasms
Papilloma
PUNLMP*
Malignant neoplasms
Urothelial carcinoma
Squamous cell carcinoma
Adenocarcinoma
Metastases
Small cell or neuroendocrine carcinoma
Carcinoid
Melanoma
Nonepithelial neoplasms
Benign neoplasms
Leiomyoma
Paraganglioma
Fibroma
Plasmacytoma
Hemangioma
Solitary fibrous tumor
Neurofibroma
Lipoma
Malignant neoplasms
Rhabdomyosarcoma
Leiomyosarcoma
Lymphoma
Osteosarcoma
Angiosarcoma
Malignant fibrous histiocytoma

*PUNLMP = papillary urothelial neoplasm of low malignant potential.

There is significant overlap in the clinical features and radiologic findings of bladder tumors, with most requiring biopsy to make a definitive diagnosis. However, there are some tumors with more specific findings, which may help direct the clinical evaluation. This article reviews the clinical, radiologic, and pathologic features of the most common epithelial and mesenchymal bladder neoplasms.

Urothelial Carcinoma

Urothelial (transitional cell) cancer is the most common urinary tract cancer in the United States and Europe, with a stable incidence in men over the past 2 decades but a slight increase in women (1). New cases in 2005 are estimated at 63,210 with 13,180 projected deaths (5). This is a disease of older patients, most being older than 65 years, but is not restricted to these groups. Of the new cases, 3.1% occur in patients under the age of 44 years and 8% occur in patients aged 45–54 years (6). Both the incidence and mortality increase with advancing age. After the age of 80 years, bladder cancer is twice as likely to develop and cause death than in those aged 60–65 years.

Bladder cancer is more common in men than in women, with a male-to-female ratio of 3–4:1; however, in women it is diagnosed at a more advanced stage and has a higher mortality rate than in men. Survival of female patients at 5 years is 78%, equal to the 10-year survival for men. Although urothelial cancer is less than half as common in black men, they have a higher mortality rate than white men. However, the death rate is declining in all groups, with the 5-year survival rate currently at 82% overall (5).

Patient symptoms are all nonspecific. The most common presenting symptom is gross hematuria, although microscopic hematuria may be detected at urinalysis. Patients may also experience voiding symptoms such as frequency, dysuria, and pelvic pain and pressure.

The pathogenesis for urothelial tumors is direct prolonged contact of the bladder urothelium with urine containing excreted carcinogens, predominantly from cigarette smoking. Smokers have four times the risk of bladder cancer, related to both the duration and amount of smoking. Cigarette smoking accounts for one-third to one-half of all cases of bladder cancer (7). The risk of developing a urothelial tumor decreases with the cessation of smoking. Smoking pipes and cigars is not as strongly associated.

There is also a well-documented causal link between urothelial cancer and a variety of occupational and environmental chemicals, including beta-naphthylamines (such as 2-naphthylamine, 4-aminobiphenyl, and benzidine) (1). Other risk factors include bladder stones, chronic infection and irritation, as well as drugs such as phenacetin and cyclophosphamide, and arsenic in drinking water. Occupational exposure to hair dyes is also believed to increase the risk of bladder cancer, but personal exposure is not (2,8,9). On a metabolic level, slow acetylators are at higher risk than fast acetylators (2). Decreased fluid intake, saccharin, tea, and coffee have not been proved to be associated with bladder cancer (2).

Figure 2. Diverticular tumor. Axial CT image shows a urothelial tumor (arrow) within a bladder diverticulum. Urinary stasis occurs with bladder diverticula, thus predisposing them to tumor development.

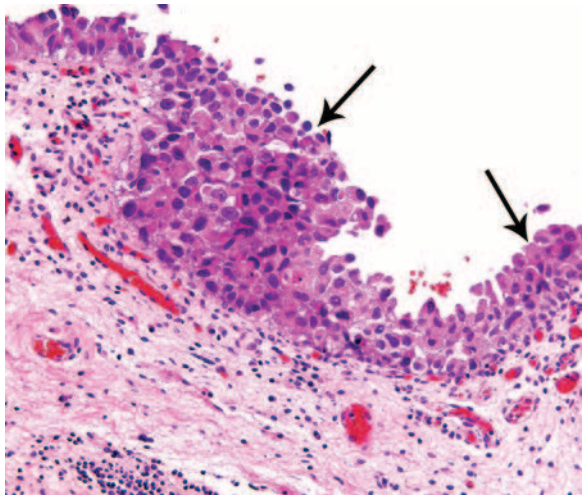

Figure 3. Urothelial carcinoma in situ. Photomicrograph (original magnification, ×100; hematoxylin-eosin stain) shows the normal urothelial lining replaced by irregular cells (arrows) with marked nuclear anaplasia and loss of cell polarity. There is no invasion into the underlying lamina propria.

Bladder diverticula have an increased risk (2%–10%) of developing cancer because of stasis. All major epithelial types have been reported, but urothelial cancer is the most common neoplasm in bladder diverticula (Fig 2) (1). Tumors occurring in diverticula have a propensity to invade perivesical fat early because of the lack of muscle in their wall.

Most urothelial tumors are located at the bladder base (80% at initial diagnosis); 60% are single, and over 50% measure less than 2.5 cm at cystoscopy. They can be papillary, sessile, or nodular. Sessile lesions include reactive urothelial hyperplasia, atypia, dysplasia, and carcinoma in situ (10). Carcinoma in situ is a noninvasive high-grade lesion with significant anaplastic change within the urothelium and cytologically malignant cells (Fig 3). It accounts for 1%–3% of urothelial neoplasms and may progress to invasive carcinoma. Sessile lesions are more likely to invade muscle; however, the prognosis correlates more with tumor grade than with morphology (ie, papillary vs flat). Most invasive tumors are high-grade carcinoma (1).

Papillary lesions include papilloma, inverted papilloma, papillary urothelial neoplasm of low malignant potential (PUNLMP), and low-grade and high-grade papillary urothelial carcinoma. PUNLMP is a relatively recent addition to the World Health Organization classification (10). It is a low-grade, small, solitary neoplasm that neither invades nor metastasizes (Fig 4). Distinction from low-grade carcinoma may be difficult and subjective. Since approximately 35% of PUNLMPs recur and 11% progress in grade, surveillance is required (10).

Seventy percent of patients have superficial papillary tumors, which have a "frond-like" appearance at cystoscopy (Fig 5). The majority have a prolonged clinical course with multiple recurrences responding to local resection, without progression to malignancy. Twenty percent of tumors are aggressive and invasive de novo, and 10% are metastatic at presentation. Twenty percent of patients with initially noninvasive tumors develop progression, and 12% die of bladder cancer (11). Predictors of behavior include depth of invasion, multiplicity, history of prior tumors, tumor size, and grade in decreasing order of importance (2).

Teaching Point

Urothelial carcinoma has a propensity to be multicentric with synchronous and metachronous bladder and upper tract tumors (Fig 6) (1). Multicentric bladder tumors occur in up to 30%–40% of cases (Fig 7) (1,12).

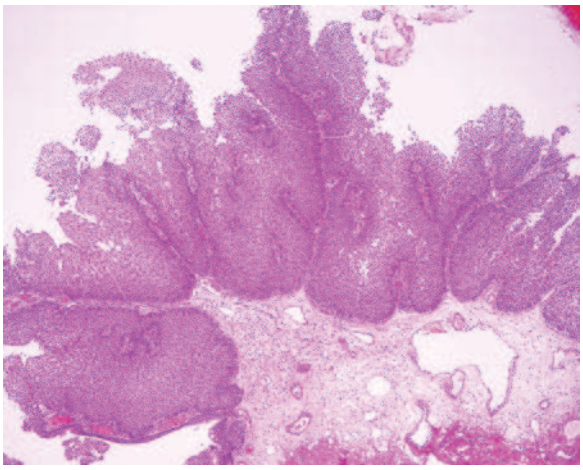

Figure 4. Papillary urothelial neoplasm of low malignant potential. Photomicrograph (original magnification, ×100; hematoxylin-eosin stain) shows papillary fronds lined by thickened urothelium without cellular atypia.

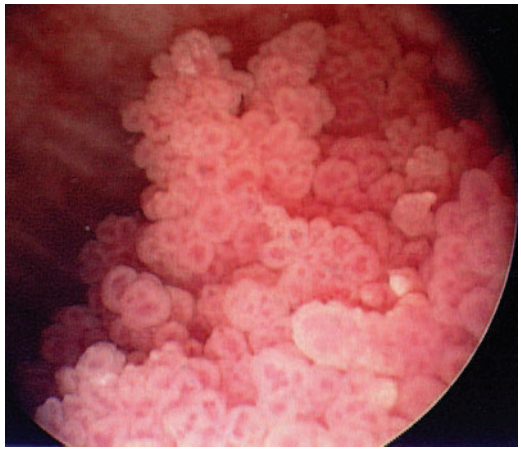

Figure 5. Papillary urothelial carcinoma. Cystoscopic photograph shows a frondlike mass fungating into the bladder lumen.

6.

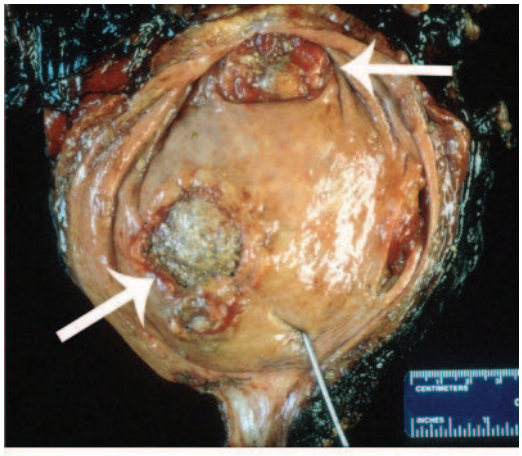

7.

Figures 6, 7. Multicentric urothelial carcinoma. **(6)** Anteroposterior radiograph obtained during retrograde pyelography shows irregular filling defects in both the bladder (straight arrow) and the renal pelvis (curved arrows). **(7)** Photograph of the bladder shows multiple synchronous tumors (arrows).

Upper tract tumors occur in 2.6%–4.5% of bladder tumor cases and are seen most frequently when multiple bladder lesions are present (13,14).

Pathologic stage is the most important predictor of survival. The TNM classification from the American Joint Committee on Cancer, a modification of the Jewett-Strong staging system, is in

Table 2
Jewett-Strong and TNM Staging Systems for Bladder Cancer

Jewett-Strong System	TNM System	Histopathologic Findings
O	T0	No tumor
O	Tis	Carcinoma in situ
O	Ta	Papillary tumor confined to the epithelium (mucosa)
A	T1	Tumor invades subepithelial connective tissue (lamina propria)
B1	T2a	Tumor invades superficial muscle (inner half)
B2	T2b	Tumor invades deep muscle (outer half)
C	T3	Tumor invades perivesical fat
D1	T4a	Tumor invades surrounding organs
D1	T4b	Tumor invades pelvic or abdominal wall
D1	N1	Metastasis in a single pelvic lymph node ≤2 cm
D1	N2	Metastasis in a single pelvic lymph node >2 cm and ≤5 cm or in multiple nodes ≤5 cm
D1	N3	Metastasis in a single lymph node >5 cm
D2	N4	Lymph node metastases above the bifurcation of the common iliac arteries
D2	M1	Distant metastases

widespread use (Table 2) (15). Superficial bladder cancer is confined to the mucosa and lamina propria. Once extension occurs into the detrusor muscle layer, the tumor is considered invasive (Fig 8). Invasion may progress to involve local organs including the prostate, vagina, uterus, and pelvic wall. Tumors metastasize most commonly to pelvic lymph nodes, then distant metastases occur in the lung, liver, and bone in decreasing order of frequency.

The standard imaging work-up for gross hematuria and suspected urothelial tumor has shifted from excretory urography to cross-sectional modalities such as ultrasonography (US), CT, and magnetic resonance (MR) imaging. Cystoscopy and biopsy are the standard of reference for bladder evaluation, but imaging is important for accurate staging and treatment planning. Superficial tumors may not be evident with any imaging study and are not staged radiologically. However, with invasive urothelial tumors, detection of pelvic side wall invasion or lymphadenopathy is critical, as clinical staging is inaccurate. Furthermore, complete evaluation of the urothelial tract (both upper and lower) is indicated because of the propensity for multicentric disease.

US may be used for initial evaluation of hematuria but is rarely the definitive test, given its limitations in the demonstration of muscle invasion and lymph node status. Most tumors appear as a papillary, hypoechoic mass or area of focal wall thickening (Fig 9). Doppler imaging will show flow within the mass, aiding in differentiation of tumor from blood clot.

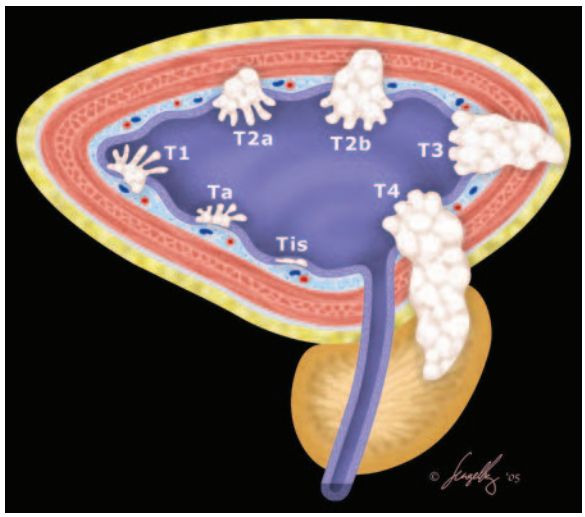

Figure 8. Diagram shows the stages of tumor invasion in bladder cancer. Tumors are considered superficial if they do not extend beyond the lamina propria (T1 or less). Once the muscle layer (muscularis propria) has been invaded (T2a or greater), the tumor is considered invasive.

At CT or CT urography, urothelial carcinoma appears as an intraluminal papillary or nodular mass (Fig 10) or focal wall thickening (Fig 11). Lesions may be missed without adequate bladder distention, especially small, flat tumors. CT demonstrates tumoral calcification in approximately 5% of cases (16). The calcification typically encrusts the surface of the tumor and may be nodular or arched (16). Bladder tumors enhance early (Fig 11), approximately 60 seconds from injection, and may be readily detected with multidetector CT. In one series of 20 patients, 100% of tumors were detected (17). With progression of

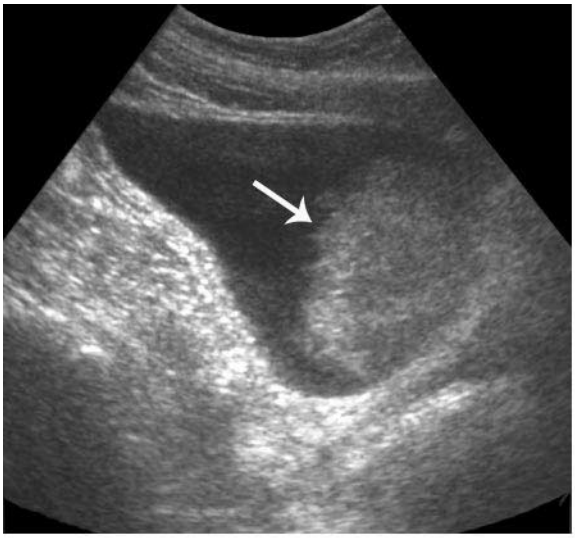

9.

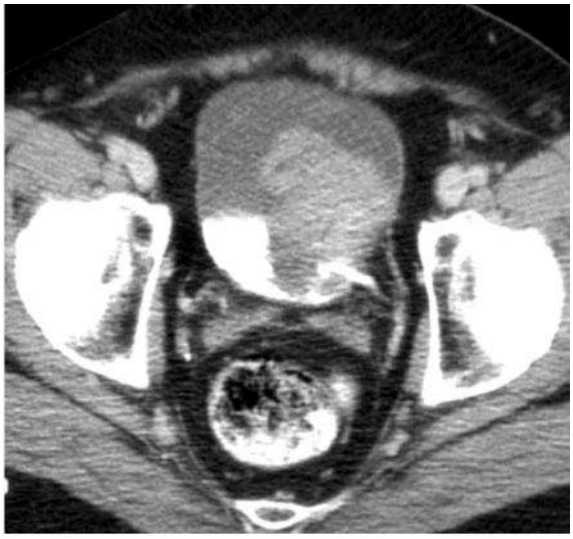

10.

11.

12.

Figures 9–12. Urothelial carcinoma. **(9)** Longitudinal US image of the bladder shows a large, hypoechoic urothelial carcinoma (arrow) within the bladder. **(10)** Axial CT image shows a large, lobular mass within the bladder. **(11)** Axial CT image of the bladder shows an enhancing area of focal wall thickening (arrow), which represents a urothelial carcinoma. Flat lesions are more difficult to detect with radiologic studies, especially if the bladder lumen is not well distended. **(12)** Axial CT image of the bladder shows a large urothelial carcinoma. There is irregular soft-tissue stranding (arrows) from tumor invasion into the perivesical fat.

disease, wall thickening may become diffuse. The presence of ureteral obstruction strongly suggests the presence of muscle invasion. Once the tumor has extended into the perivesical fat, increased attenuation or infiltration is noted in the fat (Fig 12).

After transurethral bladder tumor resection, focal wall thickening and perivesical fat stranding may mimic tumor and deep invasion, resulting in overstaging. Optimally, CT should be delayed for at least 7 days to improve specificity. Accuracy for staging of primary tumor with CT has ranged from 40% to 85% (18). Sensitivity and specificity for detecting perivesical invasion with multidetector CT are improved over those of conventional CT, at 92% and 98% respectively, with an accuracy of 96%, if performed more than 7 days after biopsy (17).

Technical improvements in MR imaging such as surface coils, three-dimensional sequences, and fast dynamic imaging have improved spatial and temporal resolution and MR accuracy. The high intrinsic contrast of MR imaging permits distinction of bladder wall layers (18). On T1-weighted images, urine is dark; the bladder wall and tumor are intermediate in signal intensity. As fat is high in signal intensity, T1-weighted sequences are optimal for detection of extravesical infiltration, nodes, and bone metastases. Tumor is intermediate

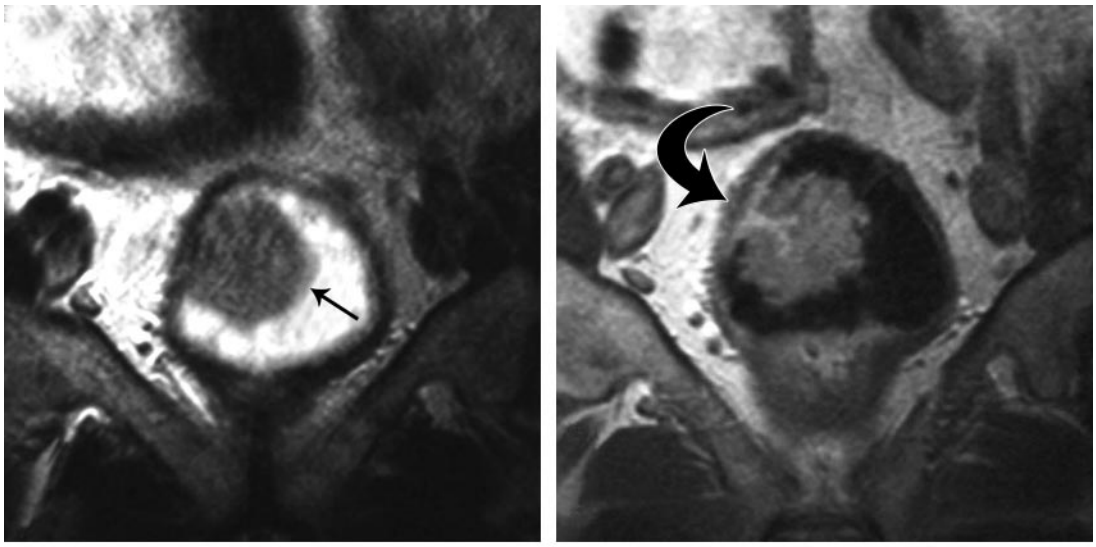

a. b.

Figure 13. Noninvasive papillary urothelial tumor. **(a)** Coronal T2-weighted MR image shows an intermediate-signal-intensity mass (arrow) within the bladder lumen. The hypointense bladder wall is intact. **(b)** Coronal early phase gadolinium-enhanced dynamic T1-weighted MR image shows that the tumor enhances more than the bladder wall (arrow).

in signal intensity on T2-weighted images, contrasting with the high signal intensity of urine and low signal intensity of muscle (Fig 13a). T2-weighted sequences are optimal for evaluation of tumor depth and differentiating tumor from fibrosis and for detection of invasion of surrounding organs and marrow metastases (18).

With fast dynamic contrast-enhanced imaging, bladder cancer enhances more avidly and earlier than other tissues such as normal bladder and postbiopsy changes (Figs 13, 14) (19). This may enable differentiation of tumor from fibrosis or edema, although this is still difficult soon after transurethral resection. MR imaging has a reported staging accuracy of 72%–96% for the primary tumor and is superior to CT for differentiation of superficial versus deep muscle invasion (18,20). However, as with CT, inflammation can mimic perivesical fat invasion and result in overstaging (20).

Metastatic lymph nodes have no specific appearance on T1- or T2-weighted images but enhance early, simultaneously with the bladder cancer. A limitation of both CT and MR imaging is the detection of metastasis in normal-sized lymph nodes, with comparable accuracy reported (21). Improved MR detection of pathologic lymph nodes (sensitivity, 96%; specificity, 95%; and negative predictive value, 98%) has been achieved with an intravenous suspension of ultrasmall iron particles, ferumoxtran-10 (21). Ferumoxtran is taken up by macrophages in lymph nodes and causes loss of signal in normal nodes on T2*-weighted images. In metastatic nodes, tumor replaces normal macrophages, preventing uptake of the iron particles and maintaining high nodal signal intensity. Distant metastases may be evaluated with either MR imaging or CT, with MR imaging superior to CT for detection of bone marrow involvement.

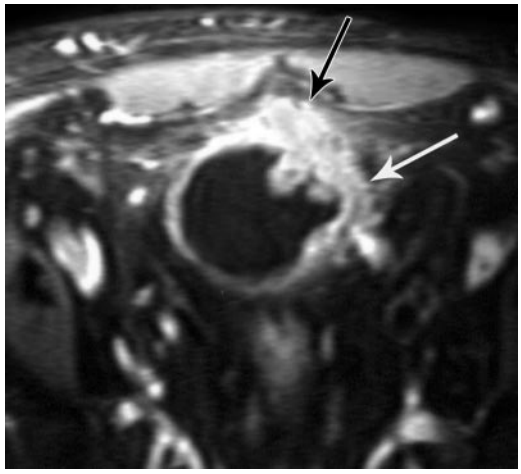

Figure 14. Invasive urothelial carcinoma. Axial gadolinium-enhanced fat-suppressed T1-weighted MR image of the bladder shows tumor invasion into the perivesical fat (arrows).

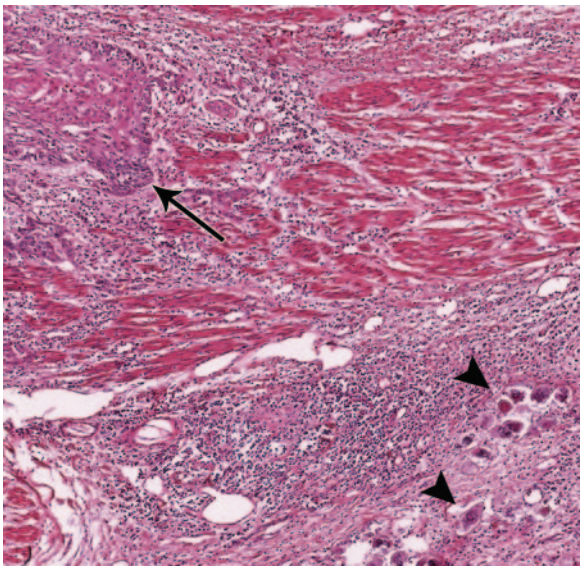

Figure 15. Squamous cell carcinoma associated with schistosomiasis. Photomicrograph (original magnification, ×100; hematoxylin-eosin stain) shows a well-differentiated squamous cell carcinoma (arrow) infiltrating the muscularis propria. Adjacent to it are *Schistosoma* eggs (arrowheads), most of which are calcified.

The usefulness of fluorine 18 fluorodeoxyglucose (FDG) positron emission tomography (PET) in bladder cancer is limited by the excretion of radioisotope into the bladder, which obscures the tumor. Irrigating the bladder with saline improves detection of bladder tumors (22). Currently, optimal use of PET or PET-CT is for detection of distant metastasis, pelvic lymph node metastasis, or pelvic recurrence and potentially to separate tumor from fibrosis or radiation change (23).

Treatment of urothelial carcinoma depends on stage and grade. Superficial tumors are treated with cystoscopic resection followed by close monitoring for recurrences. Recurrent tumors are treated with intravesical agents such as mitomycin C or bacillus Calmette-Guérin. Radical cystectomy and urinary diversion are reserved for invasive cancer. Systemic chemotherapy is used for local recurrence after surgery or to palliate metastases.

Survival is directly related to depth of invasion and presence of metastatic disease. If the tumor is confined to the lamina propria, 5-year survival after cystectomy is 55%–80% (11). The 5-year survival drops to 40% with invasion of the muscularis propria and decreases to 20% when there is invasion of perivesical fat. The 5-year survival rate for metastatic cancer is 6% (1,11).

Imaging plays a limited role in long-term surveillance. Radiation, fibrosis, and intravesical local therapy may cause wall thickening, which is difficult to distinguish from tumor. Cystoscopy with biopsy remains the standard of reference for detecting recurrence but is both invasive and expensive, especially since surveillance should be lifelong. Virtual CT cystoscopy, performed with carbon dioxide, room air, or contrast material distention of the urinary bladder, has been proposed as a noninvasive alternative to conventional cystoscopy. However, the sensitivity is poor for lesions under 5 mm (24).

Urinary cytology is noninvasive and relatively inexpensive and has been used for both tumor detection and long-term surveillance. It has high specificity (94%–99%), but the lack of sensitivity for low-grade tumors (0%–50%) is a distinct problem limiting its usefulness for surveillance (25,26). For superficial low-grade tumors, detection of DNA aneuploidy with flow cytometry or of chromosomal aberrations with the fluorescent in situ hybridization technique can improve sensitivity to 70%–73% (27).

A variety of noninvasive tests on voided or washed urine have also been developed to improve sensitivity while decreasing costs and invasiveness. These urinary markers include bladder tumor antigen, fibrin degradation product, telomerase, and nuclear matrix protein 22 (28). However, in practice there is no single ideal marker, and improved sensitivity with maintained specificity is achieved by a combination of urine cytology with use of other markers.

Squamous Cell Carcinoma

Squamous cell carcinoma accounts for less than 5% of bladder neoplasms in the United States (1). However, in parts of the world where schistosomiasis (bilharziasis) is endemic, it is a major health problem, accounting for over 50% of bladder cancers (29) (Fig 15). Patients with nonbilharzial squamous bladder carcinoma tend to present after the age of 60 years, with a slight male predominance, whereas those with bilharziasis tend to be younger and are five times more likely to be male. Symptoms include gross hematuria and irritative voiding symptoms.

Risk factors in nonbilharzial regions include chronic irritation from indwelling catheters, bladder calculi, or chronic infection. All of these risk

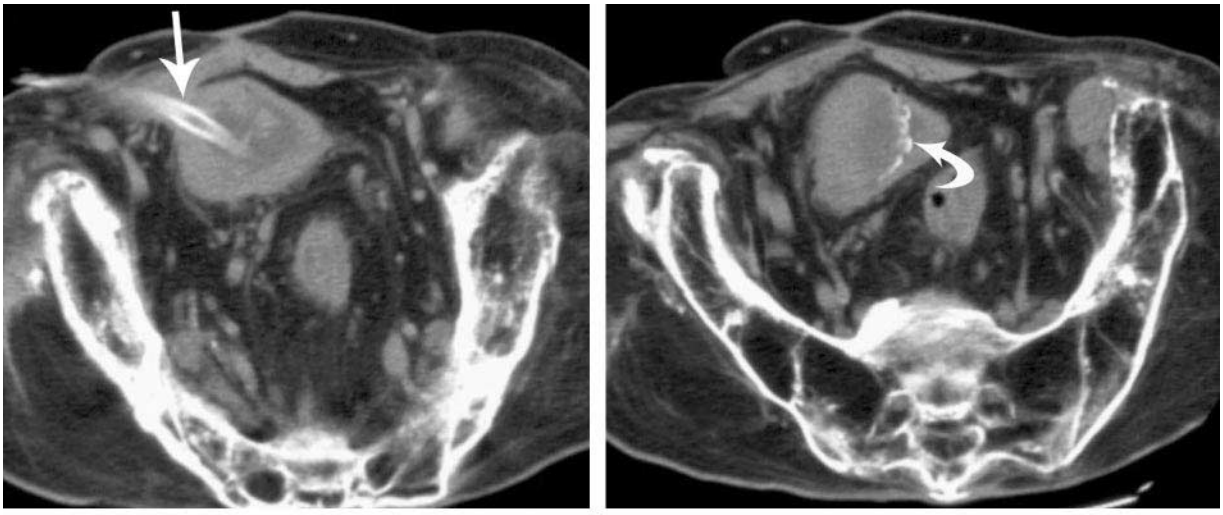

a. b.

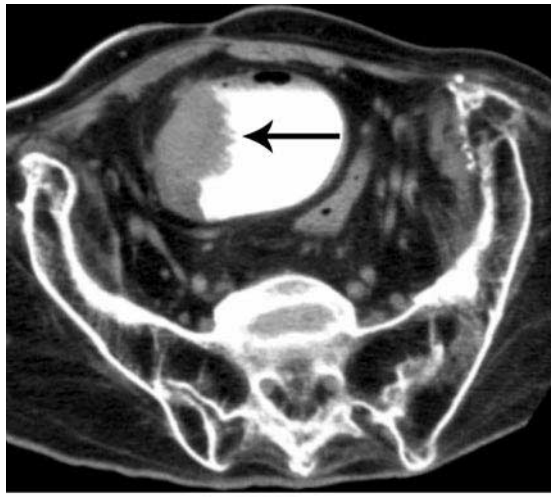

c.

Figure 16. Squamous cell carcinoma in a paraplegic patient. **(a)** Axial unenhanced CT image shows a suprapubic catheter (arrow) entering the bladder. **(b)** Axial unenhanced CT image of the bladder shows calcifications (arrow) encrusting a tumor. **(c)** Axial contrast material–enhanced CT cystogram shows the tumor (arrow) more clearly. Note the loss of trabecular structure in the bones and the fatty infiltration of the muscles.

factors may be present in paraplegic patients, putting them at increased risk (Fig 16). Cyclophosphamide has also been implicated in the pathogenesis of squamous carcinoma of the bladder, as well as smoking and intravesical bacillus Calmette-Guérin (1,30).

Cytologic findings may be confused with those of squamous metaplasia. Tumor differentiation is variable, with keratinized squamous cells and keratin pearls in well-differentiated squamous carcinoma. Tumors are high grade and locally aggressive with muscle invasion in 80% (31). There is a predilection for the trigone and lateral bladder, and the tumor may occur in bladder diverticula as well (32). At cystoscopy, squamous carcinoma is a large, often ulcerated, infiltrating mass.

The imaging findings in squamous carcinoma are nonspecific. Tumors may appear as a single enhancing bladder mass or as diffuse or focal wall thickening (33,34). Intradiverticular squamous tumors are soft-tissue masses, sometimes with surface calcification (32). In contrast to urothelial carcinoma, squamous carcinoma is sessile rather than papillary, and pure intraluminal growth is not seen. Bladder wall thickening and calcification, from chronic inflammation or infection with *Bilharzia*, may coexist and complicate the diagnosis (Fig 17). Muscle invasion is present in 80% of cases and extravesical spread may be extensive, involving surrounding organs and the abdominal wall (Fig 18) (34).

The prognosis is dependent on the local stage. Given the large percentage of patients who have extravesical extension at the time of diagnosis, the overall prognosis for squamous cell carcinoma is generally poor. Death is usually from local failure, with metastases found in only 8%–10% of cases (29). Therefore, aggressive local treatment with radical cystectomy is the treatment of choice. Given the poor prognosis, consideration should be given to screening high-risk patients with urinary cytology and cystoscopy.

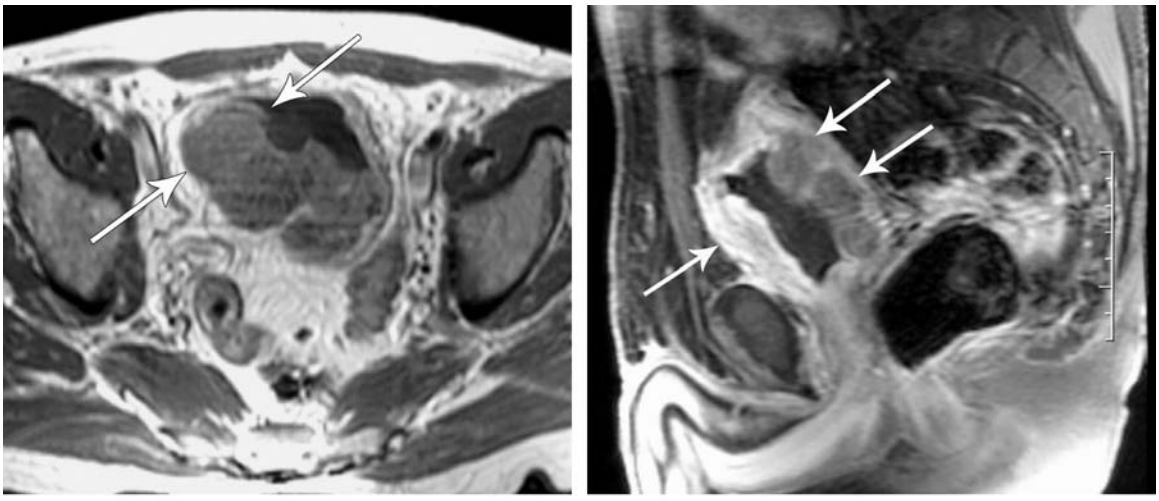

a. b.

Figure 17. Squamous cell carcinoma. **(a)** Axial T1-weighted MR image shows lobular thickening of the lateral bladder wall (arrows). **(b)** Sagittal gadolinium-enhanced fat-suppressed T1-weighted MR image shows thickening of the anterior and posterior bladder walls (arrows). Pathologic evaluation showed chronic inflammatory changes with diffuse invasive squamous cell carcinoma. Inflammatory changes may make evaluation of tumor extension difficult.

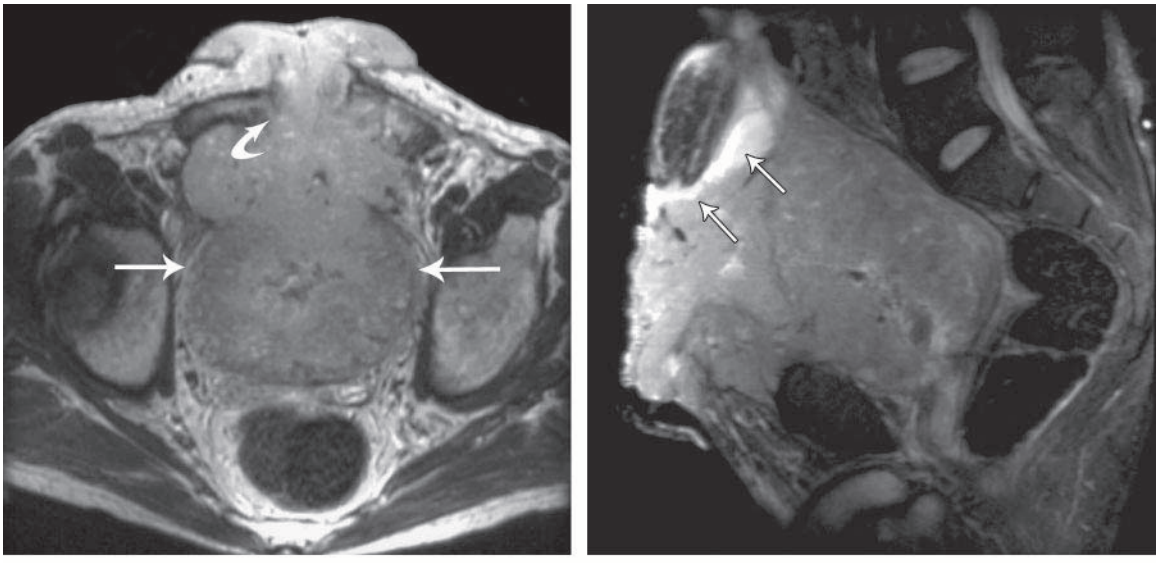

a. b.

c.

Figure 18. Invasive squamous cell carcinoma. **(a)** Axial T2-weighted MR image shows a soft-tissue mass (straight arrows) filling the pelvis and obliterating the normal bladder lumen. The mass is locally aggressive and has eroded through the abdominal wall (curved arrow). **(b)** Sagittal T2-weighted MR image shows urine tracking along the upper edge of the tumor (arrows). Urine was noted to be pooling on the patient's abdomen. **(c)** Photograph of the patient's abdomen shows the fungating mass.

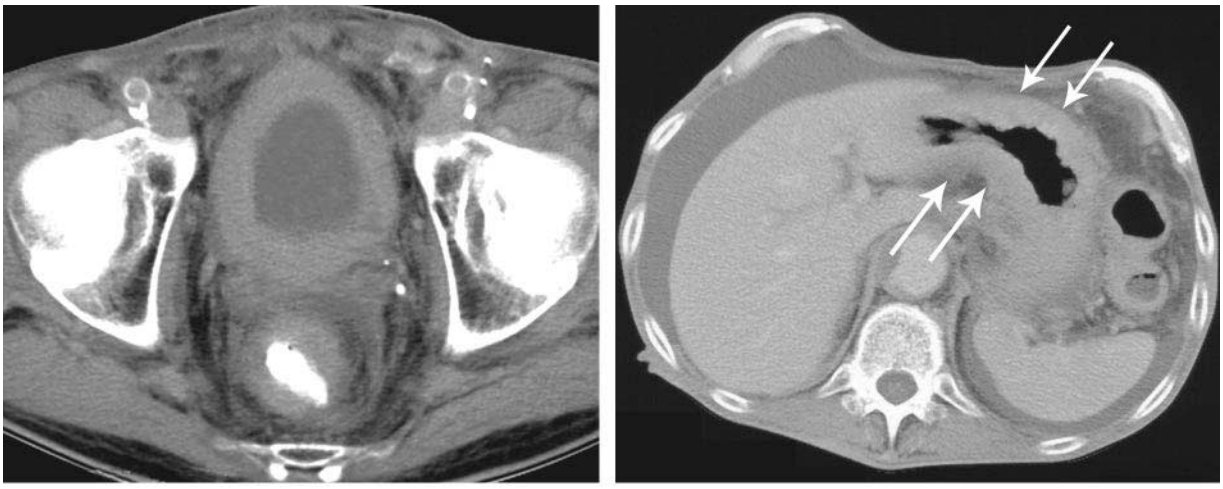

a. b.

c.

Figure 19. Adenocarcinoma. **(a)** Axial CT image shows diffuse thickening of the bladder wall. **(b)** Axial CT image of the upper abdomen shows similar thickening of the wall of the gastric antrum (arrows). Ascites is present as well. **(c)** Photograph of the bladder wall shows diffuse smooth thickening, an appearance typical of linitis plastica. Autopsy evaluation of the stomach and bladder showed adenocarcinoma; it was not possible to determine which location was the site of the primary tumor.

Adenocarcinoma

Adenocarcinoma is an uncommon bladder neoplasm representing less than 2% of bladder neoplasms (1,35). It can be subclassified as primary (two-thirds are nonurachal and one-third urachal) or secondary (metastases). The mean age at presentation for nonurachal cancer is 60 years, with urachal cancer occurring approximately 10 years earlier. Nonurachal adenocarcinoma is three times more common in men, whereas urachal adenocarcinoma occurs equally often in men and women. Patients present with hematuria in 90% of cases and irritative symptoms in 50%. Mucus may be secreted in the urine in 25% of patients with urachal adenocarcinoma (36). Urachal cancer may also manifest with an umbilical discharge.

Adenocarcinoma is classically associated with bladder exstrophy and a persistent urachus. Other risk factors for bladder adenocarcinoma include intestinal metaplasia from chronic mucosal irritation, with the risk dependent on the degree and duration of urothelial disturbance. Adenocarcinoma is also found after urinary diversions such as enterocystoplasty and has an increased prevalence in pelvic lipomatosis because of associated cystitis glandularis.

Metastatic adenocarcinoma to the bladder is more common than primary adenocarcinoma and occurs in a wider age range (37). Adenocarcinoma is the most common histologic type of secondary bladder neoplasms. The bladder can be directly invaded by adjacent pelvic neoplasms, most commonly in the colon, prostate, and rectum (37). Blood-borne or lymphatic metastases from stomach, breast, or lung cancers are less frequent. It is extremely important to distinguish primary from secondary adenocarcinoma because of different treatment options. As bladder metastases are a late manifestation of cancer, there is usually evidence of a locally invasive adjacent primary neoplasm or other signs of a distant primary neoplasm.

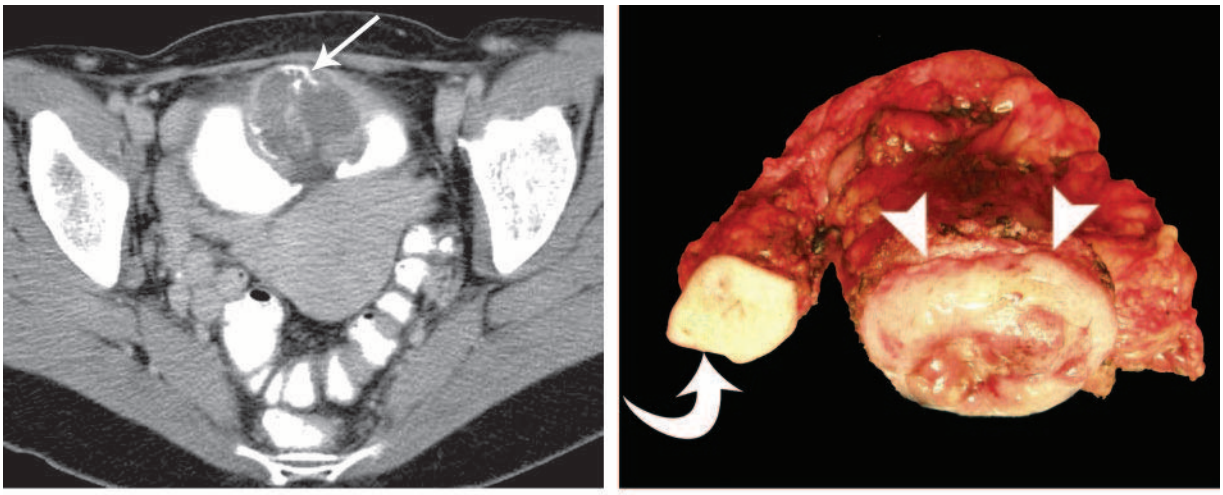

a. b.

Figure 20. Urachal adenocarcinoma. **(a)** Axial CT image shows a midline, low-attenuation, soft-tissue mass involving the dome of the bladder. Note the peripheral calcifications (arrow). **(b)** Photograph of the pathologic specimen shows that the surgical resection extended from the bladder dome mass (arrowheads) up to the umbilicus (arrow).

Urine cytology is quite specific for adenocarcinoma, and some metastatic subtypes may be readily detected (38). However, sensitivity is limited by the submucosal location of some tumors and the paucity of exfoliated cells in urine. At cystoscopy, primary adenocarcinoma is typically a single nodular lesion, with 58%–67% favoring the bladder base and the rest located in the region of the urachus. Primary adenocarcinoma may be histologically identical to colonic adenocarcinoma with subtypes such as mucinous and signet ring. Signet-ring carcinoma is usually a diffusely infiltrating process simulating linitis plastica. It may be difficult, even with special stains, to distinguish primary adenocarcinoma from metastases to the bladder (Fig 19) (37).

In a series of 14 patients with primary nonurachal adenocarcinoma, 75% had diffuse bladder wall thickening at CT (mean thickness, 1.8 cm) and 88% had stranding of the perivesical fat (39). Twenty-five percent showed lymphadenopathy, and 25% had direct invasion of the rectus muscle. A propensity to peritoneal metastases was noted (39).

Urachal adenocarcinoma is characteristically located at the dome of the bladder in the midline or slightly off midline. Ninety percent of masses occur close to the bladder, with the remainder along the course of the urachus or at the umbilical end. A midline, infraumbilical, soft-tissue mass with calcification is characteristic and is considered to be urachal adenocarcinoma until proved otherwise (Fig 20) (36). These tumors are distinguished by the prominent extravesical component compared with other, nonurachal tumors of the bladder dome. Tumors are typically large, with a mean size of 6 cm in a series of 25 cases (40).

Teaching Point

Eighty percent of urachal cancers are adenocarcinoma; the rest are urothelial or squamous cancer. As most urachal remnants are lined by transitional epithelium, adenocarcinoma is believed to arise in areas of intestinal metaplasia or from rests of embryonic hindgut epithelium within the urachus. Mucin stains are positive in 69% of urachal adenocarcinomas (36).

Excretory urography may reveal a filling defect in the dome of the bladder or extrinsic compression. The tumor may be readily detected with US as a soft-tissue mass, which may be heterogeneous and calcified. Doppler imaging may show

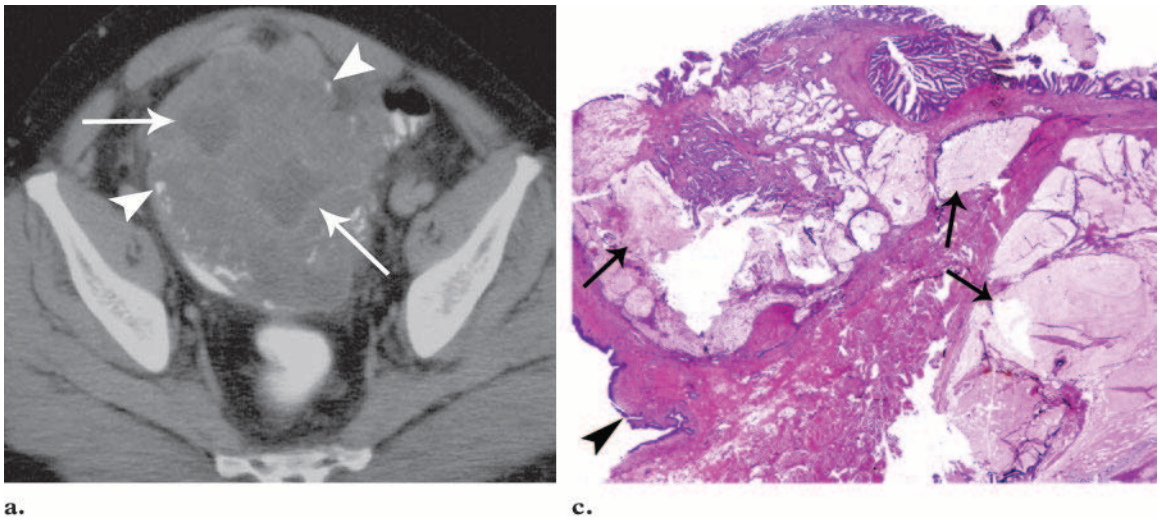

a. c. b.

Figure 21. Urachal adenocarcinoma. **(a)** Axial CT image shows a large, predominantly solid, midline mass with peripheral calcifications (arrowheads). Within the mass are scattered low-attenuation areas (arrows), which represent mucin. **(b)** Photograph of the cut surface of the tumor shows a glistening appearance. **(c)** Photomicrograph (original magnification, ×2; hematoxylin-eosin stain) shows adenocarcinoma involving the bladder wall with large lakes of mucin (arrows). The bladder mucosa (arrowhead) is normal.

internal vascularity, but this is not specific. CT and MR imaging are the most accurate modalities for local staging and for evaluation of distant metastases.

At CT, the tumor is mixed solid and cystic in 84% of cases and solid in the remainder. The cystic contents represent mucin, a common finding in these tumors (Fig 21). CT is the most sensitive modality for calcification, which is present in 72% of cases and is more commonly peripheral than stippled (40,41). Urachal carcinoma can be intraluminal, but the bulk of tumor is outside the bladder in 88% of cases (40). In contradistinction to urothelial carcinoma, extravesical spread is very common, with bladder wall invasion in 92% of cases and metastases in 48% (40,42). Rarely, pseudomyxoma peritonei may result from peritoneal carcinomatosis (Fig 22).

At MR imaging, the location of urachal carcinoma is best demonstrated on sagittal images. On T2-weighted images, focal areas of high signal intensity from mucin are highly suggestive (42). The solid portions of the tumor are isointense to soft tissue on T1-weighted images and enhance with intravenous contrast material.

Most tumors are high grade and have diffusely invaded the bladder muscle at diagnosis (1). In addition, owing to their extravesical location, urachal tumors may be clinically silent until quite large, resulting in late presentation and poor prognosis. Radical cystectomy is considered the treatment of choice for primary adenocarcinoma. For urachal adenocarcinoma, more aggressive surgery including cystectomy and en bloc resection of the urachal mass, posterior rectus fascia, peritoneum, and abdominal wall is the standard of care. Outcome is poor for invasive tumors, with an overall 20%–40% survival at 5 years (1). The prognosis is related to stage rather than histologic

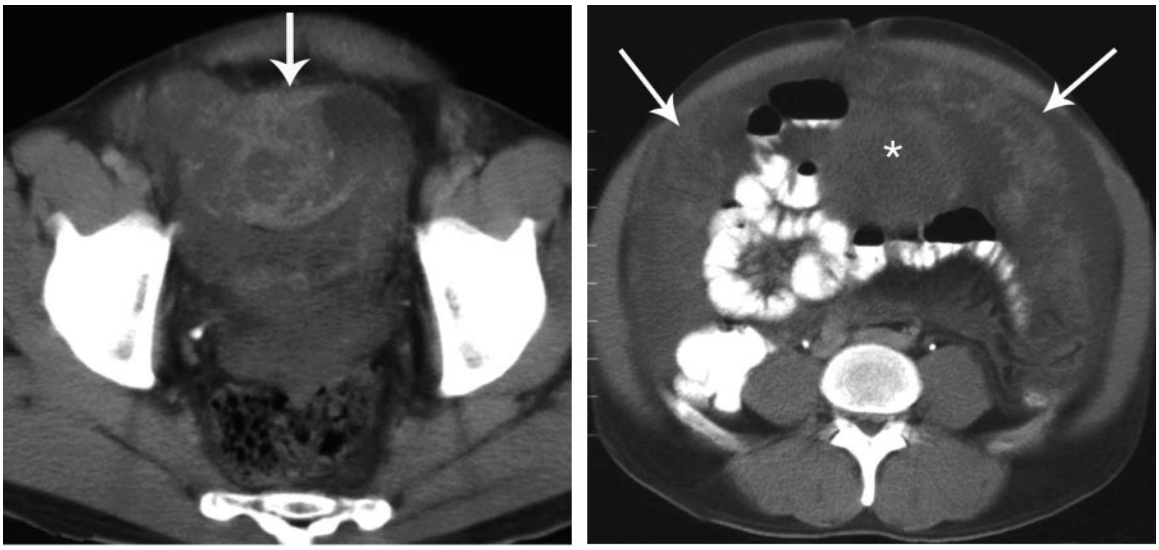

a. b.

Figure 22. Pseudomyxoma peritonei from urachal carcinoma. **(a)** Axial CT image shows a low-attenuation mass (arrow) involving the dome of the bladder. **(b)** Axial CT image of the midabdomen shows low-attenuation material and soft-tissue masses (arrows) within the peritoneal cavity. The bowel is displaced and is not free floating, as it would be in simple ascites. ∗ = top of the bladder mass.

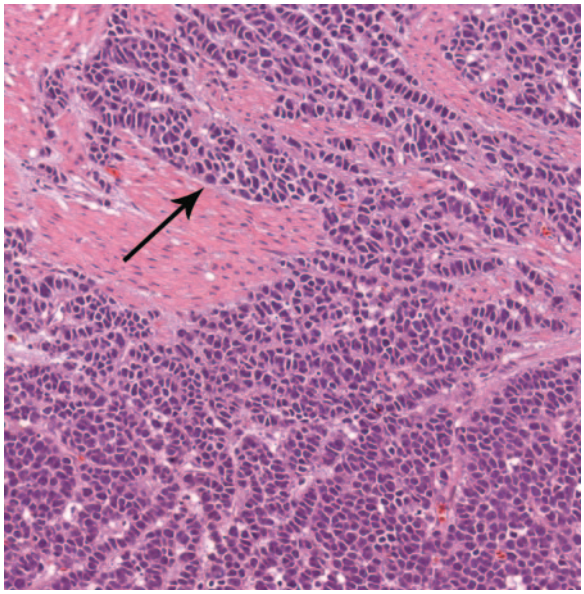

Figure 23. Small cell carcinoma. Photomicrograph (original magnification, ×100; hematoxylin-eosin stain) shows small, round cells with scant cytoplasm infiltrating the muscularis mucosa in sheets and linear cords (arrow).

subtype or location, with the exception of the signet-ring subtype, which has a 5-year survival of 13% (43).

Small Cell or Neuroendocrine Tumor

Small cell bladder tumor is rare, accounting for less than 0.5% of bladder neoplasms. They are highly aggressive tumors, with invasive disease in 94% at presentation (1,44,45). Patients present with hematuria in 88% and have a history of smoking cigarettes in 65%. The reported age range is wide, occurring in patients from 20 to 91 years, with a male-to-female ratio of 3–5:1 (44,45).

Small cell bladder tumors are believed to originate from dedifferentiated neuroendocrine cells. Histologically, they are characterized by sheets of small cells with round hyperchromatic nuclei, sparse cytoplasm, and frequent mitoses with necrosis (Fig 23). The majority of patients have mixed tumor histology, with pure small cell occurring in 32%.

Tumors are typically large and polypoid or nodular and may have an ulcerated surface. The lateral bladder walls are the most common site (45). Wall invasion is typical, with masses ranging from 3 to 8 cm. Central necrosis and cystic change may be seen with CT (46). Calcification is

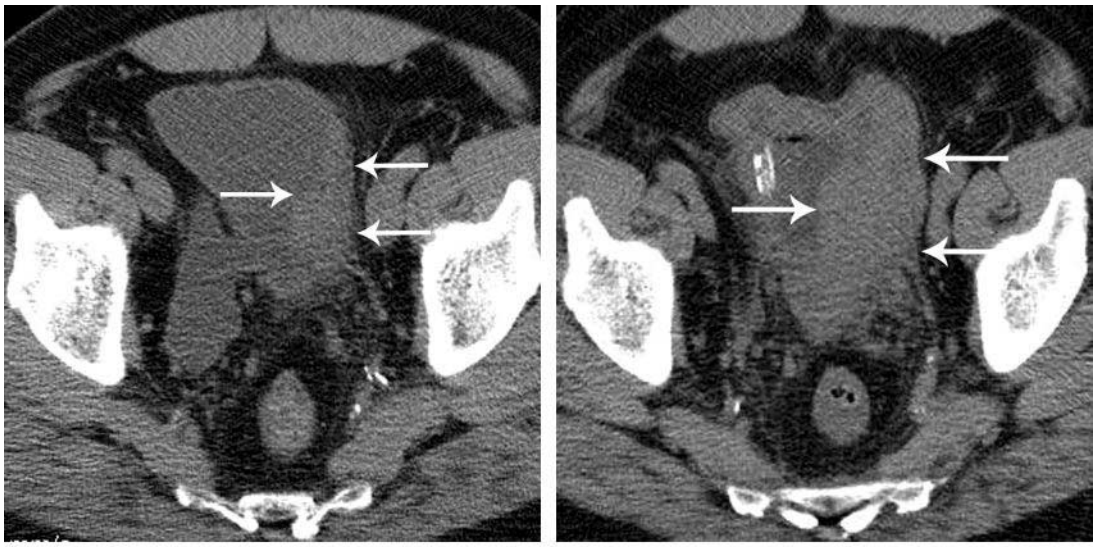

a. b.

Figure 24. Small cell carcinoma. **(a)** Axial CT image shows a mass (arrows) in the bladder wall. **(b)** Axial CT image obtained 2 weeks later shows a rapid increase in the size of the mass (arrows).

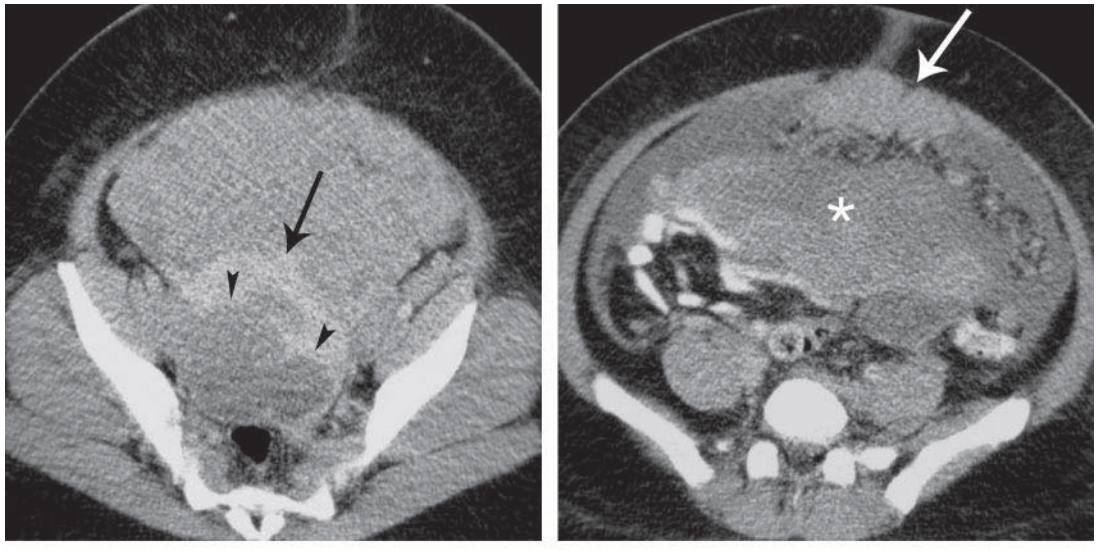

a. b.

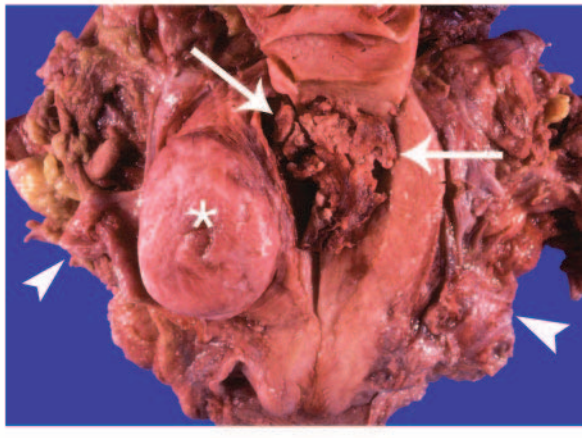

c.

Figure 25. Small cell carcinoma. **(a)** Axial CT image, obtained in a patient with small cell carcinoma of the bladder, shows a soft-tissue mass that fills the pelvis and surrounds the uterus (arrow). Note the scalloping of the posterior uterine wall (arrowheads). **(b)** Axial CT image of the midabdomen shows metastases in the omentum (arrow) and mesentery (*). **(c)** Photograph of the uterus bivalved in the coronal plane shows the surrounding tumor (arrowheads) with invasion into the endometrium (arrows). An incidental fibroid (*) is also seen.

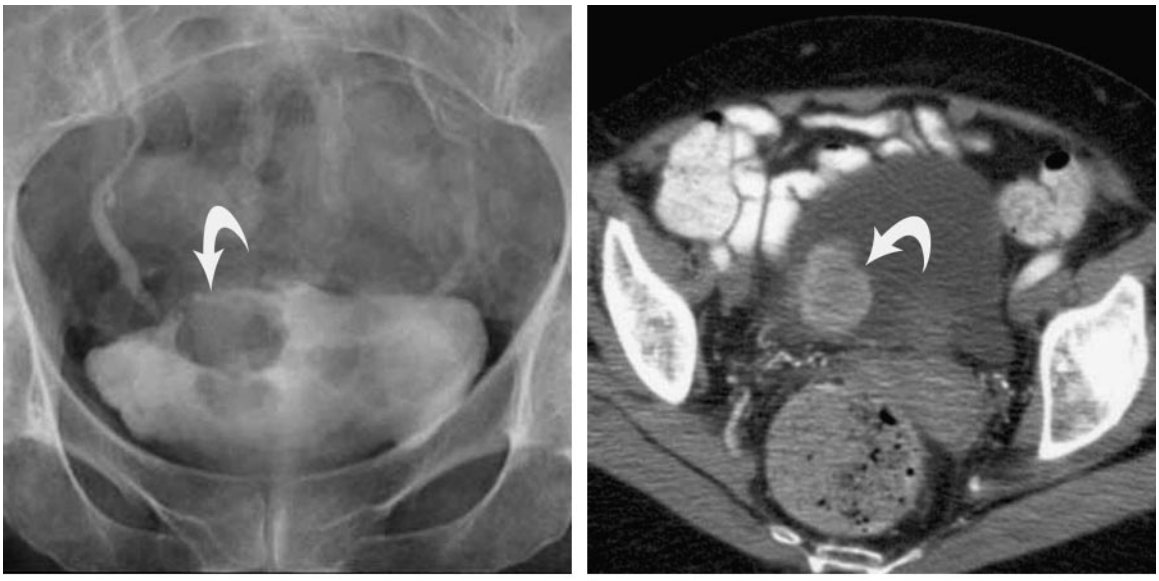

a. b.

Figure 26. Carcinoid. **(a)** Anteroposterior radiograph obtained during intravenous urography shows a polypoid filling defect (arrow) in the bladder. **(b)** Axial CT image shows the solid, polypoid, enhancing mass (arrow). The imaging characteristics are nonspecific.

uncommon. In contrast to urothelial carcinoma, tumor enhancement is patchy (47). Small cell tumors may exhibit very rapid growth (Fig 24). Aggressive behavior is further reflected in extensive local invasion, including the seminal vesicles, ureters, uterus, vagina, abdominal musculature, and diffuse peritoneal metastases (Fig 25) (44). Lymph node metastases occur in 66% of cases, with distant metastases occurring in the liver, bone, and lung (1).

Treatment consists of radical cystectomy and extended pelvic lymphadenectomy. Surgical resection alone is unlikely to be curative, unless the tumor is confined to the bladder. Combination therapy with adjuvant or neoadjuvant chemotherapy appears beneficial (48). Despite therapy, the long-term prognosis is poor, with a 16% 5-year survival (44,48).

Carcinoid

Primary carcinoid tumors are an extremely rare variant of neuroendocrine tumors and may be pure or mixed. Hematuria is the typical presenting symptom. These tumors are round or polypoid and small, with a mean size of 6 mm (49). Most are located in the bladder neck or trigone and are covered by normal epithelium. The carcinoid syndrome has not been reported from a primary bladder carcinoid, to our knowledge. Behavior is typically benign, but metastases can occur in up to 30% of cases (50). Imaging features are not specific, an intraluminal mass being the most common finding (Fig 26).

Leiomyoma

Leiomyoma is the most common mesenchymal tumor of the bladder but accounts for only 0.43% of bladder tumors (51). Leiomyomas occur equally in men and women with a wide age range of 22–78 years (52). Most are small and asymptomatic and are discovered incidentally. However, large tumors manifest with symptoms such as hesitancy, frequency, dribbling, hematuria, pressure from mass effect, or urinary obstruction (53). Histologically, leiomyomas are noninfiltrative smooth muscle tumors lacking mitotic activity, cellular atypia, and necrosis.

Leiomyomas arise in the submucosa, but growth may be submucosal (7%), intravesical (63%), or extravesical (30%) (54). At cystoscopy, normal bladder mucosa covers the leiomyoma. Imaging features include either a smooth indentation of the bladder wall or an intraluminal mass. They are smooth, solid, homogeneous masses. Cystic components indicate degeneration. MR imaging is superior in demonstrating the submucosal origin of the tumor and the preservation of the muscle layer.

Bladder leiomyomas exhibit characteristics similar to those of their uterine counterpart at US, CT, and MR imaging, with MR imaging being most specific for tissue characterization (55). Typically, leiomyomas exhibit intermediate signal intensity on T1-weighted images and low signal intensity on T2-weighted images (Fig 27).

Teaching Point

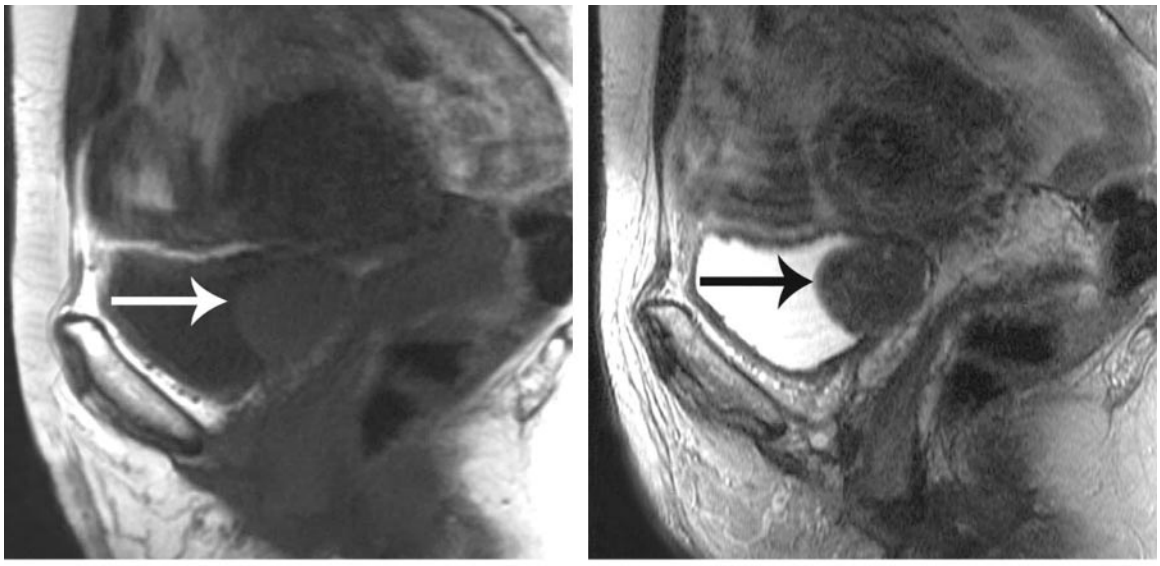

a. b.

Figure 27. Leiomyoma. Sagittal T1-weighted **(a)** and T2-weighted **(b)** MR images of the bladder show a smooth, low-signal-intensity, intramural mass (arrows), an appearance typical of a leiomyoma.

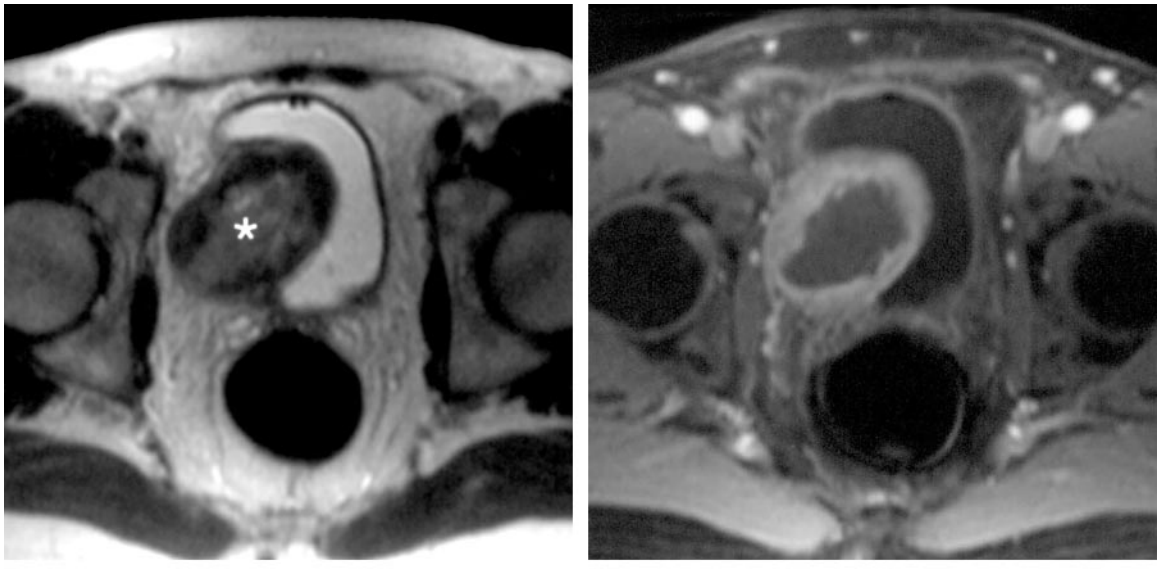

a. b.

Figure 28. Degenerated leiomyoma. **(a)** Axial T2-weighted MR image shows an intramural mass within the lateral bladder wall. The mass is well defined with a low-signal-intensity rim and a high-signal-intensity center (*). **(b)** Axial gadolinium-enhanced fat-suppressed T1-weighted MR image shows lack of enhancement in the central portion of the mass. Histologic analysis demonstrated a benign degenerated leiomyoma.

Degenerated leiomyomas have more heterogeneous signal characteristics, with cystic areas having high signal intensity on T2-weighted images (55). Contrast enhancement is variable, with degenerated areas lacking enhancement (Fig 28). A pedunculated intraluminal leiomyoma may be confused with a urothelial lesion but should be of lower signal intensity on T2-weighted images.

These are benign tumors with no malignant potential, but histologic evaluation is essential to distinguish them from a well-differentiated leiomyosarcoma. Focal excision of the mass is the treatment of choice. A preoperative suspicion of a leiomyoma is invaluable in alerting the surgeon to the benign nature of the mass and preventing unnecessary radical surgery.

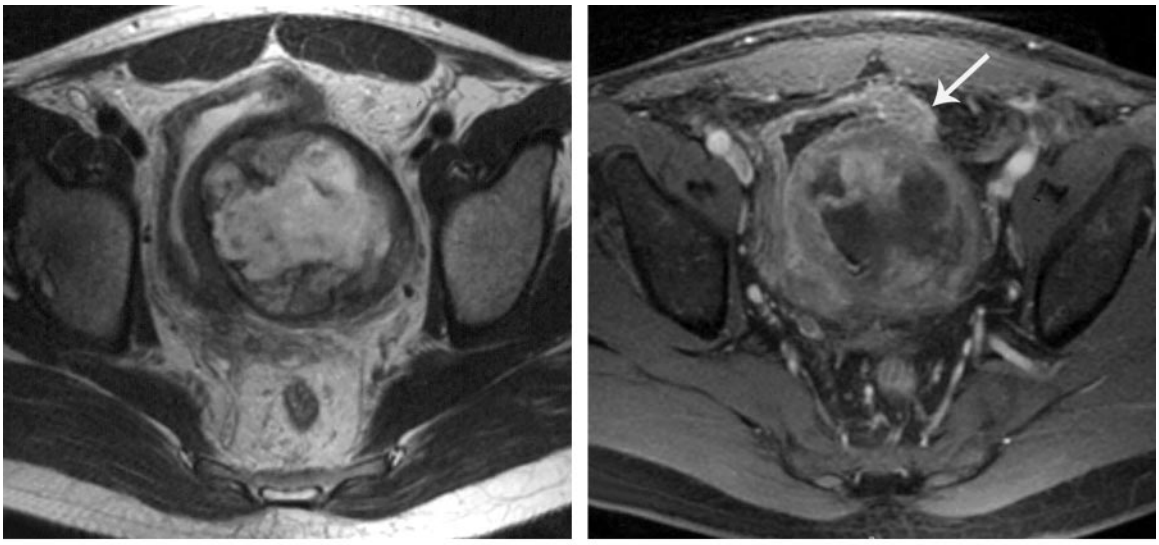

a. b.

Figure 29. Leiomyosarcoma. **(a)** Axial T2-weighted MR image shows a large, heterogeneous mass within the bladder wall. **(b)** Axial gadolinium-enhanced fat-suppressed T1-weighted MR image shows irregular enhancement of the mass. The adjacent bladder wall (arrow) is also abnormal and was found to be infiltrated by the tumor.

Leiomyosarcoma

Leiomyosarcoma is the most common nonepithelial malignant bladder tumor in adults. An increased prevalence is seen after radiation therapy or systemic chemotherapy with cyclophosphamide for another neoplasm. Patients present relatively early secondary to hematuria, and many have urinary obstruction. The age range is wide at 25–88 years with a male-to-female ratio of 3:1 (52). Eighty percent of leiomyosarcomas are high grade at presentation, although both high-grade and low-grade tumors can behave aggressively with local recurrence and distant metastases.

It can be difficult to distinguish leiomyoma from leiomyosarcoma at imaging. Both can have relatively low signal intensity on T2-weighted MR images (56). However, necrosis is common in leiomyosarcomas, which tend to be poorly circumscribed, invasive masses with a mean size of 7 cm (52). Consequently, they are more heterogeneous on T2-weighted images and demonstrate nonenhancing areas secondary to necrosis (Fig 29).

Treatment consists of radical cystectomy with resection of margins. Systemic chemotherapy is used for metastases or combined with radiation therapy prior to surgery for improved resectability. The 5-year survival rate for high-grade leiomyosarcoma is 62% (57).

Rhabdomyosarcoma

Rhabdomyosarcomas arise from primitive muscle cells and can occur anywhere in the body except bone. Within the genitourinary tract, the bladder and prostate are the most common sites, and 5% of all rhabdomyosarcomas occur in these organs. Rhabdomyosarcoma is the most common bladder tumor in patients under the age of 10 years, with a mean patient age of 4 years; it affects boys more than girls in a ratio of 3:1 (1). It is exceedingly rare in adults. Several associations can be seen with rhabdomyosarcoma, including congenital anomalies of the brain, neurofibromatosis, and nephroblastomas (1).

Children present with hematuria, dysuria, retention, or urinary tract infection. Rhabdomyosarcoma can manifest as a diffusely infiltrative lesion or as masses, which can be polypoid and "grapelike" (sarcoma botryoides). The cut surface of the tumor can be glistening, gray-white, and gelatinous with variable necrosis and hemorrhage (58,59). Ninety percent of bladder rhabdomyosarcomas are embryonal in subtype, and the rest are alveolar. All are composed of malignant spindle cells intermixed with loose, myxoid,

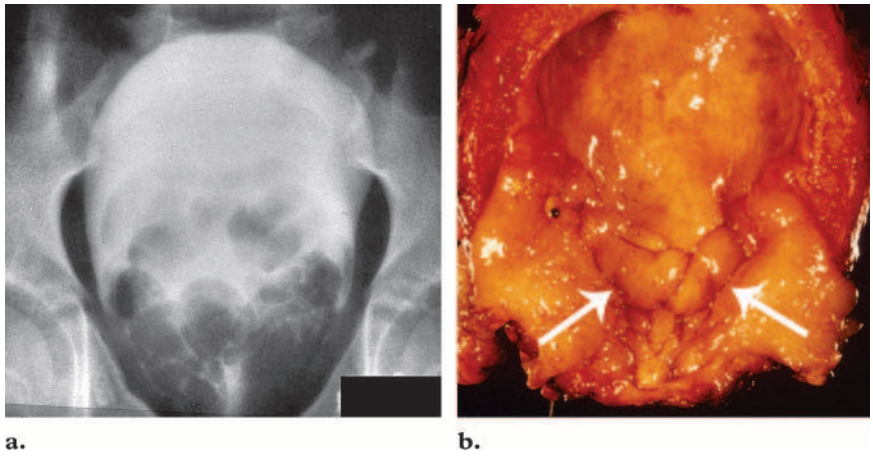

Figure 31. Botryoid rhabdomyosarcoma. **(a)** Anteroposterior radiograph obtained during intravenous urography shows multiple nodular filling defects arising from the base of the bladder. **(b)** Photograph of the cystectomy specimen shows several tumor nodules (arrows) along the posterior wall.

edematous stroma (59). A highly cellular zone (cambium layer) beneath the urothelium is typical (Fig 30).

Imaging typically shows large, nodular filling defects or masses often associated with urinary obstruction (59). These tumors often involve the bladder base, and when large, are difficult to differentiate from those originating from the prostate gland. At MR imaging, rhabdomyosarcoma has low signal intensity on T1-weighted images and high signal intensity on T2-weighted images with heterogeneous enhancement. Multiple grapelike intraluminal masses are highly suggestive of botryoid rhabdomyosarcoma (Figs 31, 32). Rhabdomyosarcoma may be locally invasive, and a significant extravesical component may be present (Fig 33). CT and MR are superior to other imaging modalities for demonstrating the extent of local invasion and lymphadenopathy.

Teaching Point

There has been a shift in treatment from surgical resection to chemotherapy. With first-line chemotherapy, the need for radical surgery has decreased and the survival rate is greater than 70% (60). Low stage, botryoid pattern, and embryonal histology are favorable prognostic factors (58).

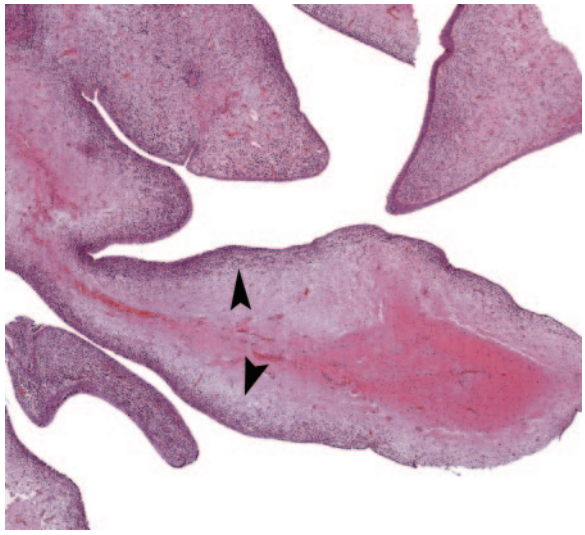

Figure 30. Sarcoma botryoides. Photomicrograph (original magnification, ×4; hematoxylin-eosin stain) shows the typical polypoid projections of tumor tissue into the bladder lumen. Note the cellular zone (cambium layer) (arrowheads) underneath the urothelial lining.

Neurofibroma

Neurofibromas of the bladder are rare, but the bladder is the most common genitourinary site of a neurofibroma. They may be isolated or occur in association with neurofibromatosis type 1 (von Recklinghausen disease). Patients most com-

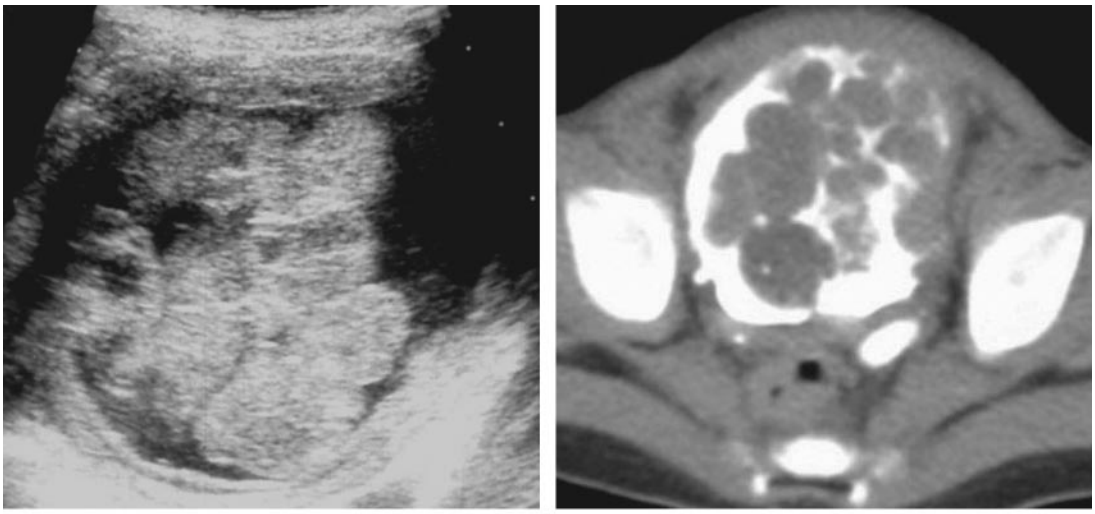

a. b.

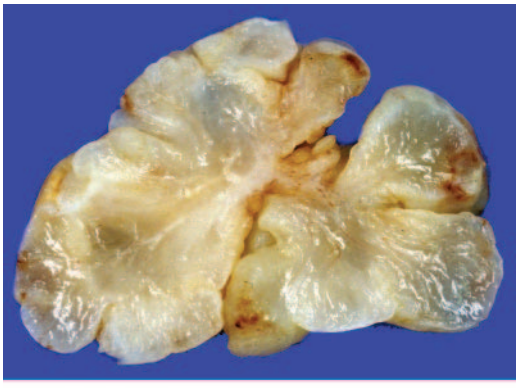

c.

Figure 32. Botryoid rhabdomyosarcoma. **(a, b)** Transverse US **(a)** and axial CT **(b)** images show a grapelike mass filling the bladder lumen. **(c)** Photograph of the cut surface of the gross specimen shows the typical grayish, glistening, gelatinous appearance of the tumors.

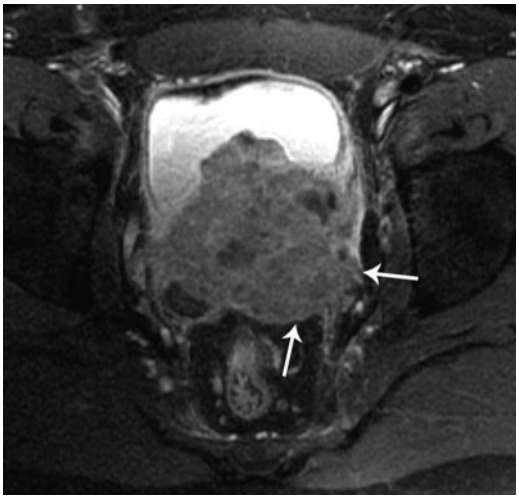

Figure 33. Invasive rhabdomyosarcoma. Axial gadolinium-enhanced fat-suppressed T1-weighted MR image of the bladder shows a tumor with significant extravesical extension (arrows).

monly present with urinary tract infections. Other symptoms include hematuria, urinary frequency and urgency, mass, or obstruction.

Neurofibromas arise from the nerve plexuses, which enter near the bladder trigone (61). Neurofibromas may be localized, diffuse, or plexiform. Plexiform neurofibromas consist of nodules on a thickened nerve and its branches, reminiscent of a bag of worms or knots on a cord. These nodules may dramatically thicken the bladder wall, obstruct the ureteral orifice, and cause hydronephrosis. The mass may also bulge into the bladder lumen. In addition, the tumor may involve the uterus, vagina, and urethra in females and the prostate, seminal vesicles, and urethra in males (61). Large tumors may surround the rectum and extend to the perineum. Malignant degeneration can occur (62).

Characteristic CT and MR imaging features are diffuse, nodular bladder wall thickening with masses extending to the pelvic side wall (63). Masses are typically low in attenuation at CT

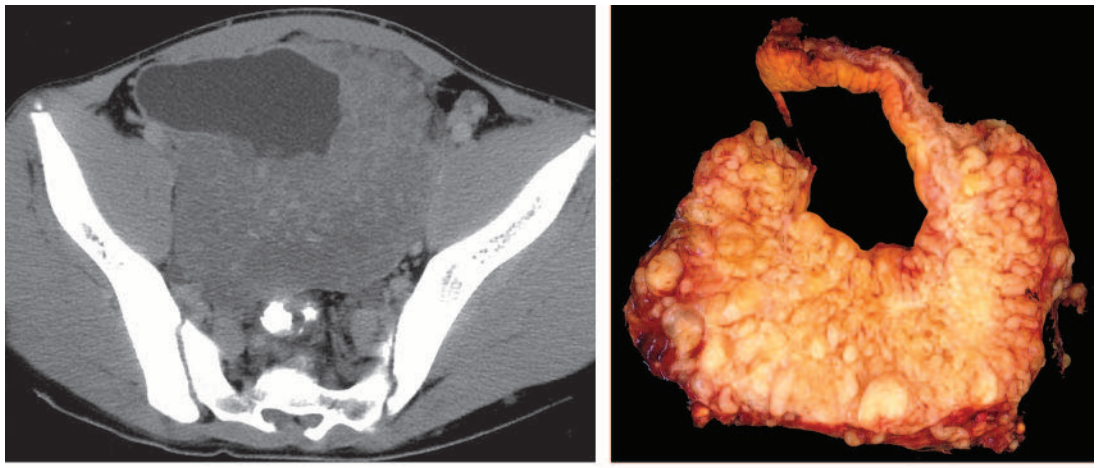

a. b.

Figure 34. Plexiform neurofibroma in a patient with known neurofibromatosis type 1. **(a)** Axial CT image shows low-attenuation, nodular thickening of the left lateral and posterior bladder walls. **(b)** Photograph of the cut surface of the resected bladder shows multiple fleshy nodules within the bladder wall.

Teaching Point

with nonuniform enhancement (Fig 34). MR imaging features are more specific, with low signal intensity on T1-weighted images (although slightly higher than that of skeletal muscle) and a target sign on T2-weighted images, which consists of low-signal-intensity fibrosis surrounded by high-signal-intensity myxoid stroma (64). This target pattern is highly suggestive of a plexiform neurofibroma (Fig 35) (64). After contrast material administration, the myxoid stroma enhances. Nodular masses extending through the pelvis into bony foramina are also highly suggestive of a plexiform neurofibroma.

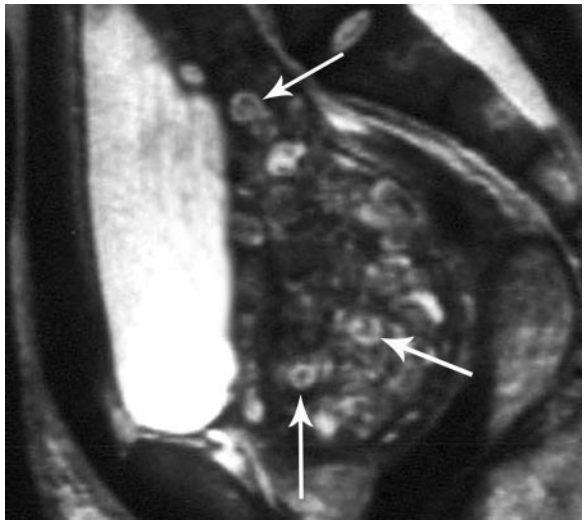

Figure 35. Plexiform neurofibroma. Sagittal T2-weighted MR image shows nodular thickening of the posterior bladder wall. Several nodules have a low-signal-intensity center surrounded by a high-signal-intensity rim (the target sign) (arrows). This sign is highly suggestive of a plexiform neurofibroma.

Paraganglioma

Paragangliomas (the preferred term for pheochromocytomas arising outside the adrenal gland) may rarely manifest as a bladder mass. They account for 0.1% of all bladder tumors and 1% of all pheochromocytomas. The age range is wide at 10–78 years, and there is a female preponderance (1). A characteristic clinical syndrome of catecholamine release during micturition, "micturition attack," occurs in 50% of patients. Symptoms include severe headache, anxiety, sweating, tremor, pounding sensation and syncope with hypertension, and increased urinary catecholamine levels. Hematuria is common. Nonfunctioning pheochromocytomas are also reported. Most are sporadic, but they can occur in the setting of a familial syndrome such as neurofibromatosis, von Hippel–Lindau syndrome, Sturge-Weber syndrome, tuberous sclerosis, or multiple endocrine neoplasia (65).

Paraganglioma arises in the chromaffin cells of the sympathetic chain in the detrusor muscle layer and may occur anywhere in the bladder. Histologic evaluation shows a characteristic nesting pattern of round cells into balls (zellballen) (Fig 36). Five percent to 18% behave in a malignant fashion, but histology is not predictive of behavior (1,66). At cystoscopy, the findings are a small, solitary, submucosal mass or nodule. Bi-

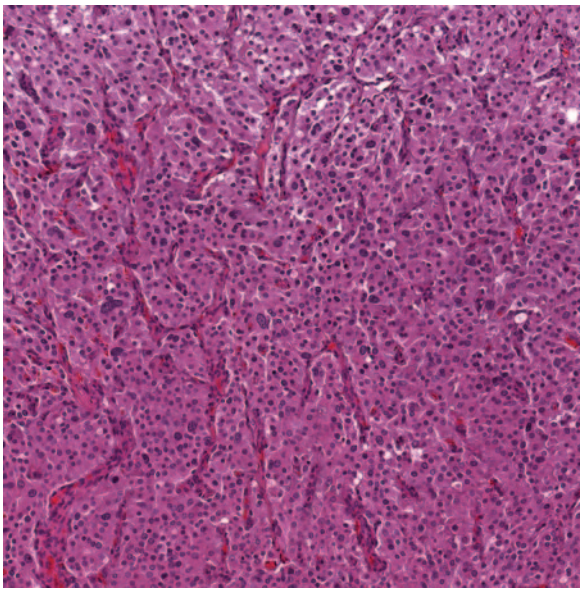

Figure 36. Paraganglioma. Photomicrograph (original magnification, ×60; hematoxylin-eosin stain) shows blood vessels compartmentalizing eosinophilic tumor cells into groups (zellballen).

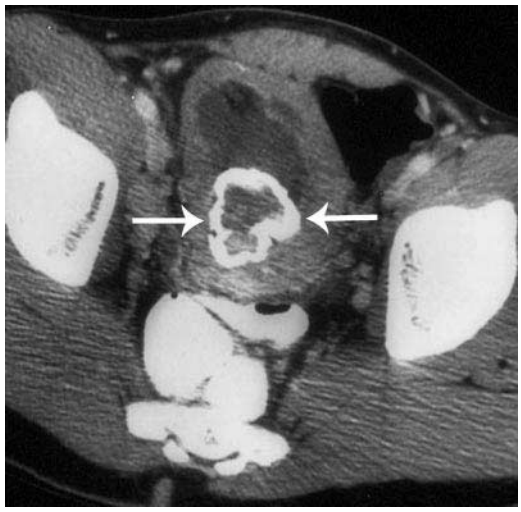

Figure 37. Paraganglioma. Axial CT image of the bladder shows dense ring calcification (arrows) around the circumference of a paraganglioma.

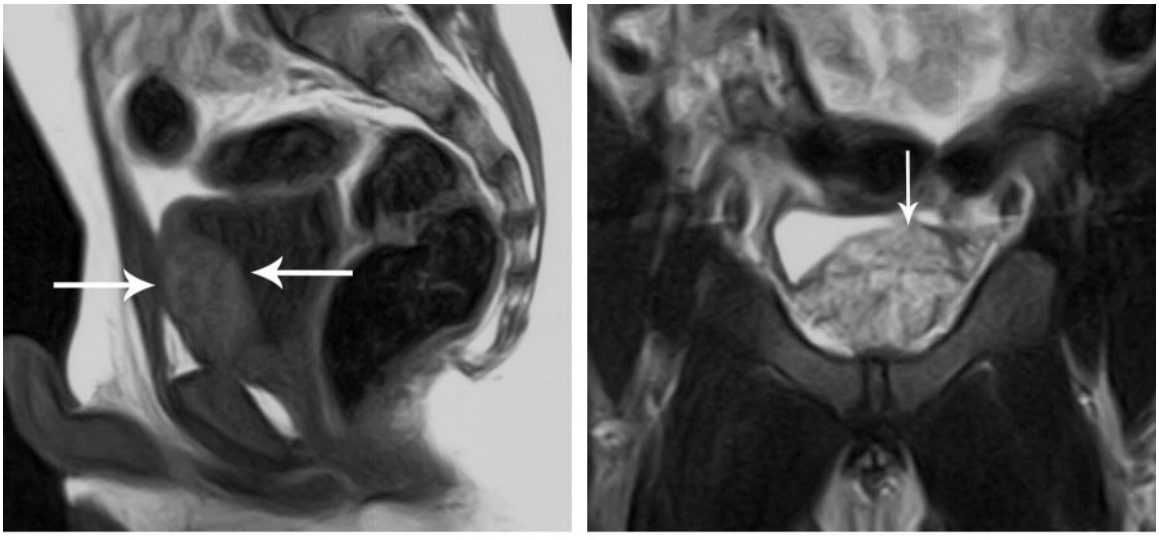

a. **b.**

Figure 38. Paraganglioma. **(a)** Sagittal T1-weighted MR image shows a low-signal-intensity submucosal mass (arrows) within the anterior bladder wall. **(b)** Coronal T2-weighted MR image shows moderately high heterogeneous signal intensity in the mass (arrow).

opsy may cause release of catecholamines and hypertensive crisis.

A bladder paraganglioma is usually a solid, homogeneous, lobulated, well-marginated mass, but cystic areas may result from necrosis or hemorrhage. A submucosal location at cross-sectional imaging and marked enhancement with either iodinated contrast material or gadolinium chelates are key features (67). Ring calcification around the circumference of the mass is highly suggestive of a bladder paraganglioma (Fig 37) (68). They are typically of low signal intensity on T1-weighted images and moderately high signal intensity on T2-weighted images (Fig 38) (65). MR imaging is superior to CT for demonstration of the submucosal origin of the tumor.

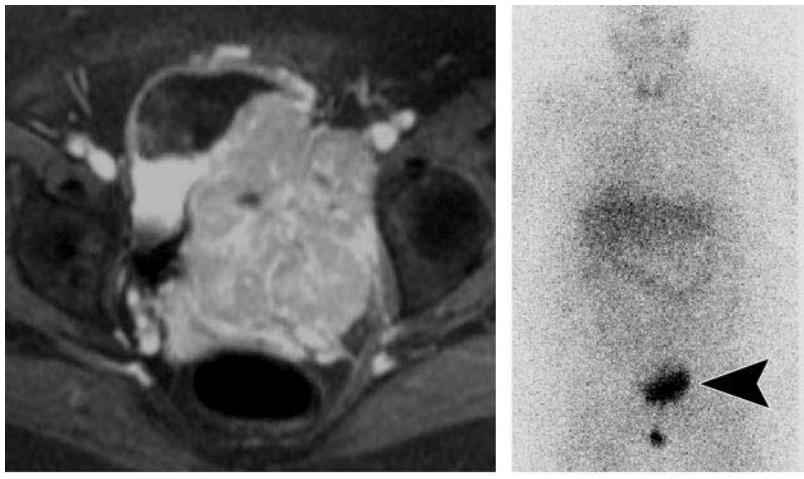

Figure 39. Paraganglioma. **(a)** Axial gadolinium-enhanced fat-suppressed T1-weighted MR image shows a large bladder mass with significant extravesical extension. This appearance is nonspecific and may be seen with many tumors. **(b)** Frontal ^{131}I-MIBG scan shows uptake in the mass (arrowhead), a finding that is highly specific for a paraganglioma.

Iodine 131 (^{131}I) metaiodobenzylguanidine (MIBG) scanning is highly specific (96%) for paragangliomas (Fig 39). However, MR imaging is more sensitive than either ^{131}I-MIBG scanning or CT (88% sensitivity for MR imaging compared to 64% for ^{131}I-MIBG scanning and 64% for CT in extraadrenal lesions) (69). PET with 6-[18F] fluorodopamine (an analogue of dopamine) may be superior to MIBG scanning in identifying metastatic lymph nodes (70).

Treatment consists of local excision following adrenergic blockade, with lymphadenectomy if the lesion is invasive. Because there are no reliable histologic criteria to distinguish benign from malignant tumors, long-term follow-up is advisable.

Lymphoma

Primary bladder lymphoma is rare, as there is no lymphoid tissue in the bladder, but secondary involvement of the bladder may be present in 10%–25% of patients with lymphoma and leukemia (71). It is most common in middle-aged women who may have nonspecific urinary symptoms, hematuria, or a mass. At cystoscopy or imaging, there are well-defined bladder masses at the dome or lateral walls rather than diffuse infiltration (Fig 40) (71). The masses may mimic urothelial carcinoma. Cell type is either the low-grade B-cell mucosa-associated lymphoid tissue (MALT) type or diffuse large B-cell type (71). Hodgkin lymphoma is exceedingly rare. The prognosis is good as most tumors are low grade. Treatment can be with chemotherapy or local radiation therapy (48).

Hemangioma

Bladder hemangiomas can occur at any age, but half manifest in childhood, in keeping with the congenital origin of these tumors. In adults, the mean age is 58 years (range, 19–76 years) and they are more common in males in a ratio of 3.7:1 (72). Painless gross hematuria is the most common presentation. Hemangiomas may either occur in isolation or be associated with syndromes such as Klippel-Trénaunay-Weber or Sturge-Weber.

In one of the largest reported series of 19 patients, the tumors were small, with a median size of 0.7 cm (range, 0.2–3 cm) (72). Most were single, broad-based, sessile bladder masses on the posterolateral walls. The finding of a lobulated bluish red lesion at cystoscopy is highly suggestive, but endometriosis, melanoma, and sarcoma can have a similar appearance.

Hemangiomas are hypervascular masses at US, CT, and MR imaging (Fig 41). Either a focal, lobular, intramural mass or diffuse bladder wall thickening may be observed. The tumor has low to intermediate signal intensity on T1-weighted images and markedly high signal intensity on T2-weighted images (67). Increased activity at blood pool scintigraphy is highly suggestive (73).

The diagnosis is made with biopsy. Although there is a potential for postbiopsy bleeding, this has not been the clinical experience (72). Hemangiomas are distinguished from angiosarcoma by the lack of mitotic figures. Cavernous hemangioma is the most common type, accounting for 78% of cases, with capillary and arteriovenous types having equal rates of 10%. Hemangiomas run a benign course and are treated by biopsy with fulguration when small or by partial cystectomy.

Figure 40. B-cell lymphoma. **(a)** Longitudinal US image shows intraluminal bladder masses (white arrows) involving the posterior wall and ureteral orifice. The latter mass is causing obstruction in the form of a hydroureter (black arrows). **(b)** Axial CT image shows the thickening at the ureteral orifice (arrows). **(c)** Cystoscopic image of the right ureteral orifice shows the lobular nature of the mass. **(d)** Photomicrograph (original magnification, ×150; hematoxylin-eosin stain) shows sheets of tumor cells with large nuclei and little cytoplasm.

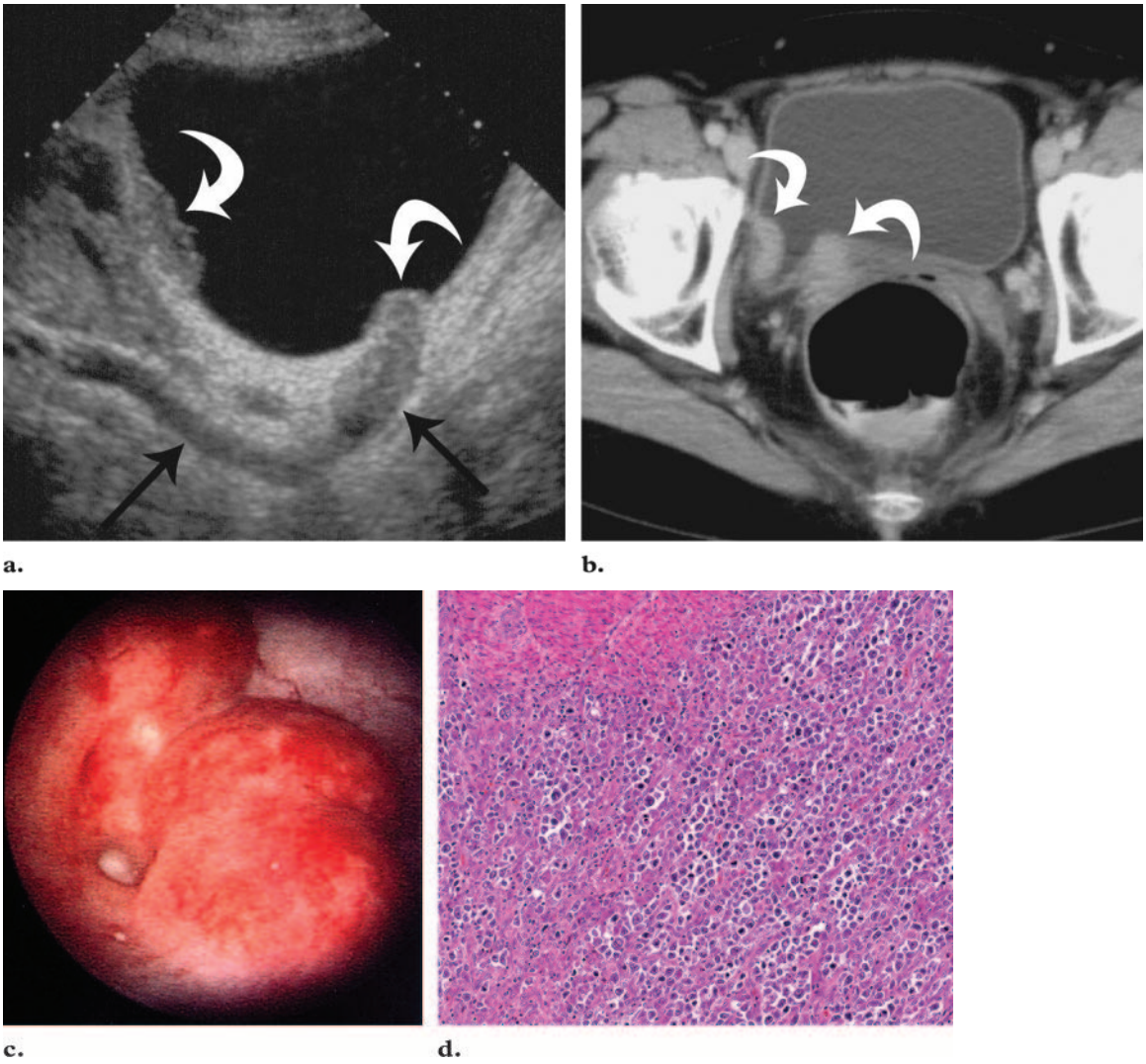

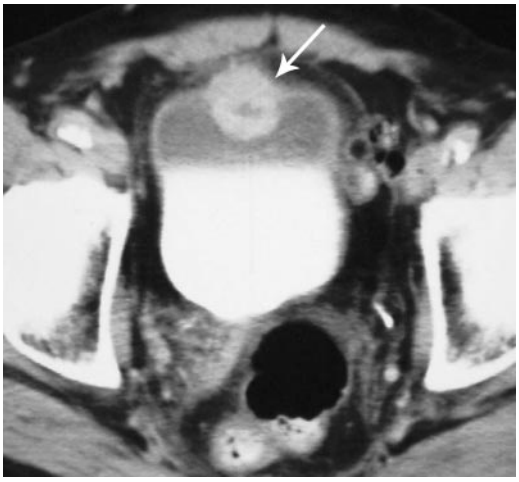

Figure 41. Hemangioma. Axial CT image shows an intramural bladder mass (arrow) with marked enhancement.

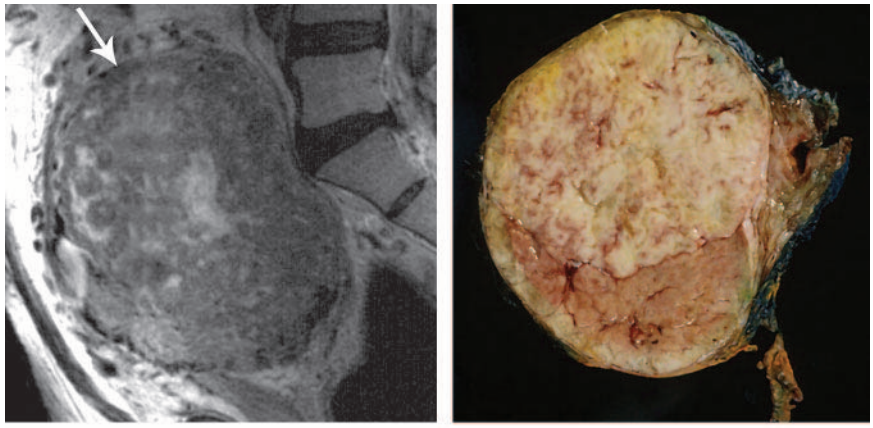

Figure 42. Solitary fibrous tumor. **(a)** Sagittal T2-weighted MR image shows obliteration of the bladder lumen by a large, predominantly low-signal-intensity mass (arrow) with scattered curvilinear areas of high signal intensity. **(b)** Photograph of the cut surface of the resected mass shows a solid, tan, fibrotic lesion, an appearance typical of solitary fibrous tumors.

Solitary Fibrous Tumor

Solitary fibrous tumors are exceedingly rare mesenchymal tumors with fibroblastic differentiation. When small, they may be detected as incidental findings. Larger tumors manifest with urinary frequency or pressure effects. More common in men, they occur in the age group of 42–67 years (74). At gross pathologic evaluation, they have a tan, whorled, fibrotic surface resembling a leiomyoma. Immunohistochemical stains are diagnostic. At CT and MR imaging, these are solid enhancing masses (75). They are typically of low signal intensity on T2-weighted images, with larger lesions exhibiting some variability (Fig 42). They are treated surgically and do not recur after partial cystectomy.

Conclusions

Urothelial carcinoma is overwhelmingly the most common bladder tumor, but it is important to be aware of the other epithelial and mesenchymal tumors that can occur. There is a significant overlap in the clinical history and imaging findings of the various bladder tumors, and ultimately they all require biopsy for diagnosis. However, some tumors such as botryoid rhabdomyosarcoma, plexiform neurofibroma, solitary fibrous tumor, leiomyomas, and urachal adenocarcinoma have highly suggestive features, which should alert the radiologist to the diagnosis. Cross-sectional imaging plays an important role for tumor staging and directing appropriate management, with CT and MR imaging having comparable accuracies.

References

1. Murphy WM, Grignon DJ, Perlman EJ. Tumors of the kidney, bladder, and related urinary structures. Washington, DC: American Registry of Pathology, 2004; 394.
2. Pashos CL, Botteman MF, Laskin BL, Redaelli A. Bladder cancer: epidemiology, diagnosis, and management. Cancer Pract 2002;10:311–322.
3. Grossfeld GD, Carroll PR. Evaluation of asymptomatic microscopic hematuria. Urol Clin North Am 1998;25:661–676.
4. Grossfeld GD, Litwin MS, Wolf JS Jr, et al. Evaluation of asymptomatic microscopic hematuria in adults: the American Urological Association best practice policy. II. Patient evaluation, cytology, voided markers, imaging, cystoscopy, nephrology evaluation, and follow-up. Urology 2001;57:604–610.
5. Cancer facts and figures 2005 (online database). American Cancer Society Web site. http://www.cancer.org/docroot/STT/content/STT_1x_Cancer_Facts__Figures_2005.asp. Published 2005.
6. Surveillance, Epidemiology, and End Results (SEER) Program, SEER*Stat Database: Incidence—SEER 9 Regs Public-Use. Bethesda, Md: National Cancer Institute, Division of Cancer Control and Population Sciences, Surveillance Research Program, Cancer Statistics Branch, 2004.
7. Marcus PM, Hayes RB, Vineis P, et al. Cigarette smoking, N-acetyltransferase 2 acetylation status, and bladder cancer risk: a case-series meta-analysis of a gene-environment interaction. Cancer Epidemiol Biomarkers Prev 2000;9:461–467.
8. Takkouche B, Etminan M, Montes-Martinez A. Personal use of hair dyes and risk of cancer: a meta-analysis. JAMA 2005;293:2516–2525.
9. Zeegers MP, Kellen E, Buntinx F, van den Brandt PA. The association between smoking, beverage consumption, diet and bladder cancer: a systematic literature review. World J Urol 2004;21:392–401.
10. Montironi R, Lopez-Beltran A. The 2004 WHO classification of bladder tumors: a summary and commentary. Int J Surg Pathol 2005;13:143–153.
11. Reuter VE. Bladder: risk and prognostic factors—a pathologist's perspective. Urol Clin North Am 1999;26:481–492.
12. Tekes A, Kamel IR, Imam K, Chan TY, Schoenberg MP, Bluemke DA. MR imaging features of transitional cell carcinoma of the urinary bladder. AJR Am J Roentgenol 2003;180:771–777.

13. Huguet-Perez J, Palou J, Millan-Rodriguez F, Salvador-Bayarri J, Villavicencio-Mavrich H, Vicente-Rodriguez J. Upper tract transitional cell carcinoma following cystectomy for bladder cancer. Eur Urol 2001;40:318–323.
14. Millan-Rodriguez F, Chechile-Toniolo G, Salvador-Bayarri J, Huguet-Perez J, Vicente-Rodriguez J. Upper urinary tract tumors after primary superficial bladder tumors: prognostic factors and risk groups. J Urol 2000;164:1183–1187.
15. Eble JN, Sauter G, Epstein JI, Sesterhenn IA, eds. Pathology and genetics of tumours of the urinary system and male genital organs. World Health Organization Classification of Tumours. Lyon, France: IARC Press, 2004.
16. Moon WK, Kim SH, Cho JM, Han MC. Calcified bladder tumors: CT features. Acta Radiol 1992; 33:440–443.
17. Kim JK, Park SY, Ahn HJ, Kim CS, Cho KS. Bladder cancer: analysis of multi-detector row helical CT enhancement pattern and accuracy in tumor detection and perivesical staging. Radiology 2004;231:725–731.
18. Barentsz JO, Witjes JA, Ruijs JH. What is new in bladder cancer imaging. Urol Clin North Am 1997;24:583–602.
19. Barentsz JO, Engelbrecht M, Jager GJ, et al. Fast dynamic gadolinium-enhanced MR imaging of urinary bladder and prostate cancer. J Magn Reson Imaging 1999;10:295–304.
20. Tekes A, Kamel I, Imam K, et al. Dynamic MRI of bladder cancer: evaluation of staging accuracy. AJR Am J Roentgenol 2005;184:121–127.
21. Deserno WM, Harisinghani MG, Taupitz M, et al. Urinary bladder cancer: preoperative nodal staging with ferumoxtran-10-enhanced MR imaging. Radiology 2004;233:449–456.
22. Kosuda S, Kison PV, Greenough R, Grossman HB, Wahl RL. Preliminary assessment of fluorine-18 fluorodeoxyglucose positron emission tomography in patients with bladder cancer. Eur J Nucl Med 1997;24:615–620.
23. Schoder H, Larson SM. Positron emission tomography for prostate, bladder, and renal cancer. Semin Nucl Med 2004;34:274–292.
24. Song JH, Francis IR, Platt JF, et al. Bladder tumor detection at virtual cystoscopy. Radiology 2001; 218:95–100.
25. Planz B, Synek C, Robben J, Bocking A, Marberger M. Diagnostic accuracy of DNA image cytometry and urinary cytology with cells from voided urine in the detection of bladder cancer. Urology 2000;56:782–786.
26. Lotan Y, Roehrborn CG. Sensitivity and specificity of commonly available bladder tumor markers versus cytology: results of a comprehensive literature review and meta-analyses. Urology 2003;61: 109–118.
27. Glas AS, Roos D, Deutekom M, Zwinderman AH, Bossuyt PM, Kurth KH. Tumor markers in the diagnosis of primary bladder cancer: a systematic review. J Urol 2003;169:1975–1982.
28. Dey P. Urinary markers of bladder carcinoma. Clin Chim Acta 2004;340:57–65.
29. Shokeir AA. Squamous cell carcinoma of the bladder: pathology, diagnosis and treatment. BJU Int 2004;93:216–220.
30. Stein JP, Skinner EC, Boyd SD, Skinner DG. Squamous cell carcinoma of the bladder associated with cyclophosphamide therapy for Wegener's granulomatosis: a report of 2 cases. J Urol 1993;149:588–589.
31. Serretta V, Pomara G, Piazza F, Gange E. Pure squamous cell carcinoma of the bladder in western countries: report on 19 consecutive cases. Eur Urol 2000;37:85–89.
32. Dondalski M, White EM, Ghahremani GG, Patel SK. Carcinoma arising in urinary bladder diverticula: imaging findings in six patients. AJR Am J Roentgenol 1993;161:817–820.
33. Narumi Y, Sato T, Hori S, et al. Squamous cell carcinoma of the uroepithelium: CT evaluation. Radiology 1989;173:853–856.
34. Wong JT, Wasserman NF, Padurean AM. Bladder squamous cell carcinoma. RadioGraphics 2004;24:855–860.
35. Grignon DJ, Ro JY, Ayala AG, Johnson DE, Ordonez NG. Primary adenocarcinoma of the urinary bladder: a clinicopathologic analysis of 72 cases. Cancer 1991;67:2165–2172.
36. Sheldon CA, Clayman RV, Gonzalez R, Williams RD, Fraley EE. Malignant urachal lesions. J Urol 1984;131:1–8.
37. Bates AW, Baithun SI. Secondary neoplasms of the bladder are histological mimics of nontransitional cell primary tumours: clinicopathological and histological features of 282 cases. Histopathology 2000;36:32–40.
38. Bardales RH, Pitman MB, Stanley MW, Korourian S, Suhrland MJ. Urine cytology of primary and secondary urinary bladder adenocarcinoma. Cancer 1998;84:335–343.
39. Hughes MJ, Fisher C, Sohaib SA. Imaging features of primary nonurachal adenocarcinoma of the bladder. AJR Am J Roentgenol 2004;183: 1397–1401.
40. Thali-Schwab CM, Woodward PJ, Wagner BJ. Computed tomographic appearance of urachal adenocarcinomas: review of 25 cases. Eur Radiol 2005;15:79–84.
41. Brick SH, Friedman AC, Pollack HM, et al. Urachal carcinoma: CT findings. Radiology 1988; 169:377–381.
42. Rafal RB, Markisz JA. Urachal carcinoma: the role of magnetic resonance imaging. Urol Radiol 1991; 12:184–187.
43. Grignon DJ, Ro JY, Ayala AG, Johnson DE. Primary signet-ring cell carcinoma of the urinary bladder. Am J Clin Pathol 1991;95:13–20.
44. Cheng L, Pan CX, Yang XJ, et al. Small cell carcinoma of the urinary bladder: a clinicopathologic analysis of 64 patients. Cancer 2004;101:957–962.
45. Sved P, Gomez P, Manoharan M, Civantos F, Soloway MS. Small cell carcinoma of the bladder. BJU Int 2004;94:12–17.
46. Kim JC, Kim KH, Jung S. Small cell carcinoma of the urinary bladder: CT and MR imaging findings. Korean J Radiol 2003;4:130–135.
47. Kim JC. CT features of bladder small cell carcinoma. Clin Imaging 2004;28:201–205.

48. Dahm P, Gschwend JE. Malignant non-urothelial neoplasms of the urinary bladder: a review. Eur Urol 2003;44:672–681.
49. Martignoni G, Eble JN. Carcinoid tumors of the urinary bladder: immunohistochemical study of 2 cases and review of the literature. Arch Pathol Lab Med 2003;127:e22–e24.
50. Hemal AK, Singh I, Pawar R, Kumar M, Taneja P. Primary malignant bladder carcinoid: a diagnostic and management dilemma. Urology 2000; 55:949.
51. Binsaleh S, Corcos J, Elhilali MM, Carrier S. Bladder leiomyoma: report of two cases and literature review. Can J Urol 2004;11:2411–2413.
52. Martin SA, Sears DL, Sebo TJ, Lohse CM, Cheville JC. Smooth muscle neoplasms of the urinary bladder: a clinicopathologic comparison of leiomyoma and leiomyosarcoma. Am J Surg Pathol 2002;26:292–300.
53. Cornella JL, Larson TR, Lee RA, Magrina JF, Kammerer-Doak D. Leiomyoma of the female urethra and bladder: report of twenty-three patients and review of the literature. Am J Obstet Gynecol 1997;176:1278–1285.
54. Knoll LD, Segura JW, Scheithauer BW. Leiomyoma of the bladder. J Urol 1986;136:906–908.
55. Sundaram CP, Rawal A, Saltzman B. Characteristics of bladder leiomyoma as noted on magnetic resonance imaging. Urology 1998;52:1142–1143.
56. Mallampati GK, Siegelman ES. MR imaging of the bladder. Magn Reson Imaging Clin N Am 2004;12:545–555.
57. Rosser CJ, Slaton JW, Izawa JI, Levy LB, Dinney CP. Clinical presentation and outcome of high-grade urinary bladder leiomyosarcoma in adults. Urology 2003;61:1151–1155.
58. Nigro KG, MacLennan GT. Rhabdomyosarcoma of the bladder and prostate. J Urol 2005;173: 1365.
59. Agrons GA, Wagner BJ, Lonergan GJ, Dickey GE, Kaufman MS. Genitourinary rhabdomyosarcoma in children: radiologic-pathologic correlation. RadioGraphics 1997;17:919–937.
60. Schalow EL, Broecker BH. Role of surgery in children with rhabdomyosarcoma. Med Pediatr Oncol 2003;41:1–6.
61. Levy AD, Patel N, Dow N, Abbott RM, Miettinen M, Sobin LH. Abdominal neoplasms in patients with neurofibromatosis type 1: radiologic-pathologic correlation. RadioGraphics 2005;25:455–480.
62. Riccardi VM. Type 1 neurofibromatosis and the pediatric patient. Curr Probl Pediatr 1992;22:66–106.
63. Shonnard KM, Jelinek JS, Benedikt RA, Kransdorf MJ. CT and MR of neurofibromatosis of the bladder. J Comput Assist Tomogr 1992;16:433–438.
64. Wilkinson LM, Manson D, Smith CR. Plexiform neurofibroma of the bladder. RadioGraphics 2004;24(Spec Issue):S237–S242.
65. Crecelius SA, Bellah R. Pheochromocytoma of the bladder in an adolescent: sonographic and MR imaging findings. AJR Am J Roentgenol 1995;165: 101–103.
66. Doran F, Varinli S, Bayazit Y, Bal N, Ozdemir S. Pheochromocytoma of the urinary bladder. APMIS 2002;110:733–736.
67. Chen M, Lipson SA, Hricak H. MR imaging evaluation of benign mesenchymal tumors of the urinary bladder. AJR Am J Roentgenol 1997;168: 399–403.
68. Asbury WL Jr, Hatcher PA, Gould HR, Reeves WA, Wilson DD. Bladder pheochromocytoma with ring calcification. Abdom Imaging 1996;21: 275–277.
69. Jalil ND, Pattou FN, Combemale F, et al. Effectiveness and limits of preoperative imaging studies for the localisation of pheochromocytomas and paragangliomas: a review of 282 cases. French Association of Surgery (AFC), and The French Association of Endocrine Surgeons (AFCE). Eur J Surg 1998;164:23–28.
70. Hwang JJ, Uchio EM, Patel SV, Linehan WM, Walther MM, Pacak K. Diagnostic localization of malignant bladder pheochromocytoma using 6-18F fluorodopamine positron emission tomography. J Urol 2003;169:274–275.
71. Bates AW, Norton AJ, Baithun SI. Malignant lymphoma of the urinary bladder: a clinicopathological study of 11 cases. J Clin Pathol 2000;53:458–461.
72. Cheng L, Nascimento AG, Neumann RM, et al. Hemangioma of the urinary bladder. Cancer 1999;86:498–504.
73. Ishikawa K, Saitoh M, Chida S. Detection of bladder hemangioma in a child by blood-pool scintigraphy. Pediatr Radiol 2003;33:433–435.
74. Kim SH, Cha KB, Choi YD, Cho NH. Solitary fibrous tumor of the urinary bladder. Yonsei Med J 2004;45:573–576.
75. Leite KR, Srougi M, Miotto A, Camara-Lopes LH. Solitary fibrous tumor in bladder wall. Int Braz J Urol 2004;30:406–409.

This article meets the criteria for 1.0 credit hour in category 1 of the AMA Physician's Recognition Award. To obtain credit, see accompanying test at http://www.rsna.org/education/rg_cme.html.

Neoplasms of the Urinary Bladder: Radiologic-Pathologic Correlation

Jade J. Wong-You–Cheong, MD, et al

RadioGraphics 2006; 26:553–580 • **Published online** 10.1148/rg.262055172 • **Content Codes:** CT GU MR

Page 556
Urothelial carcinoma has a propensity to be multicentric with synchronous and metachronous bladder and upper tract tumors (Fig 6) (1). Multicentric bladder tumors occur in up to 30%–40% of cases (Fig 7) (1,12).

Page 565
A midline, infraumbilical, soft-tissue mass with calcification is characteristic and is considered to be urachal adenocarcinoma until proved otherwise (Fig 20) (36). These tumors are distinguished by the prominent extravesical component compared with other, nonurachal tumors of the bladder dome.

Page 569
Typically, leiomyomas exhibit intermediate signal intensity on T1-weighted images and low signal intensity on T2-weighted images (Fig 27).

Page 572
At MR imaging, rhabdomyosarcoma has low signal intensity on T1-weighted images and high signal intensity on T2-weighted images with heterogeneous enhancement. Multiple grapelike intraluminal masses are highly suggestive of botryoid rhabdomyosarcoma (Figs 31, 32).

Page 574
MR imaging features are more specific, with low signal intensity on T1-weighted images (although slightly higher than that of skeletal muscle) and a target sign on T2-weighted images, which consists of low-signal-intensity fibrosis surrounded by high-signal-intensity myxoid stroma (64). This target pattern is highly suggestive of a plexiform neurofibroma (Fig 35) (64).